Journal of
Water & Climate Change

IWA PUBLISHING

Journal of Water and Climate Change Vol 14 No 1, 38 doi: 10.2166/wcc.2022.166

Assessment of satellite precipitation products at different time scales over a cyclone prone coastal river basin in India

Sridhara Setti[a,b], Karisma Yumnam[c], Maheswaran Rathinasamy[d,*] and Ankit Agarwal[c,e]

[a] Department of Civil Engineering, MVGR College of Engineering, Vizianagaram, 535002, India
[b] Centurion University of Technology and Management, Paralakhemundi, Odisha 761200, India
[c] Department of Hydrology, Indian Institute of Technology Roorkee, Uttarakhand 247667, India
[d] Department of Civil Engineering, Indian Institute of Technology Hyderabad, Kandi 502285, India
[e] Section Hydrology, GFZ German Research Center for Geosciences, Potsdam 14473, Germany
*Corresponding Author. E-mail: maheswaran27@yahoo.co.in

ABSTRACT

Precipitation is a fundamental input for many hydrological and water management studies. With the advancement in science, a variety of satellite precipitation products are available. In this study, the ability of three satellite precipitation products (TRMM-3B42v7, PERSIANN-CDR and GPM-IMERGv6) to capture rainfall were evaluated with ground-based Indian Meteorological Department (IMD) gridded data and also by driving the Soil Water Assessment Tool (SWAT) hydrological model for a cyclone prone coastal river basin in the southeast of India. Results indicate that among the three, GPM-IMERG v6 outperformed in all the statistical metrics, followed by TRMM-3B42 v7 at different temporal scales. GPM-IMERG v6 exhibited the highest correlation coefficient (0.48) and lowest root mean square error (9.52 mm/day), followed by TRMM-3B42 v7 (CC = 0.44, RMSE = 9.58 mm/day) at daily scale. In contrast to other studies in similar regions, IMERGV6 showed better performance than the PERSIANN CDR in detection skills of low, medium and high intensity rainfall events as well as False Alarm Ratio. Hydrological evaluation of the three products using the SWAT model over the study area showed satisfactory results at daily and monthly scale during the calibration and validation period. IMERGV6 is found to have better performance in hydrological evaluation as well.

Key words: GPM-IMERG, PERSIANN-CDR, satellite precipitation products TRMM, Vamsadhara River Basin (VRB)

HIGHLIGHTS

- Evaluation of four precipitation products at different time scales.
- Abilty in capturing the extreme events in a cyclone prone region.
- IMERGV6 showed better performance than the PERSIANN CDR in detection.
- Hydrological evaluation of the three products showed satisfactory results at daily and monthly scale during the calibration and validation period.
- IMERGV6 is found to have better performance in the hydrological evaluation as well.

ABBREVIATIONS

IMD	Indian Meteorological Department
TRMM	Tropical Rainfall Measurement Mission
CMORPH	Climate Prediction CenterMORPHing
PERSIANN	Precipitation Estimation from Remotely Sensed Information using Artificial Neural Networks
CDR	Climate Data Record
IMERG	Integrated Multi-satellitE Retrievals for Global Precipitation Measurement
GSMaP	Global Satellite Mapping of Precipitation
APHRODITE	Asian Precipitation – Highly-Resolved Observational Data Integration Towards Evaluation
GPCC	Global Precipitation Climatology Centre
SWAT	Soil and Water Assessment Tool
VIC	Variable Infiltration Capacity
GXAJ	Grid-Xinanjiang model
RRI	Rainfall-Runoff-Inundation
CREST	Coupled Routing and Excess STorage

1. INTRODUCTION

Precipitation data play a vital role in many hydroclimatic applications, such as water resources development projects (Zhu *et al.* 2020), management practices (Beck *et al.* 2017; Dinku 2020; Kumar & Singh 2022), planning for hydropower, flood and drought monitoring (Tan & Santo 2018; Chen *et al.* 2020b; Singh *et al.* 2020; Suseno & Yamada 2020; Tarnavsky & Bonifacio 2020; Yu *et al.* 2020), and meteorological investigations (Mishra 2019; Niyogi *et al.* 2020; Thakur *et al.* 2020; Ojha *et al.* 2021). The accurate precipitation estimation at fine resolution is critical owing to the spatiotemporal variability of rainfall (Guntu *et al.*, 2020). Indeed, gauge-based precipitation measurement is more accurate and reliable. However, a requirement for an adequate number of stations in any region elevates the cost of installation, operation, and maintenance (Agarwal *et al.* 2018). Besides, the assumption of uniform distribution of precipitation is questionable over large areas, especially in mountainous regions (Tan & Santo 2018). Also, ground-based measurements often have missing precipitation records. The missing precipitation data must be avoided in hydrological models, as the same requires continuous precipitation data.

Nowadays, many precipitation products are available with different spatial and temporal resolutions for the globe (Maggioni *et al.* 2016). These products can be grouped as gauge-only products, only satellite products, and a combination of satellite–gauge products. In recent decades, Satellite Precipitation Products (SPPs) have provided additional benefits such as freely available data with a high spatial and temporal resolution, global coverage, cost-effective coverage of mountains and oceanic regions, and, more importantly, uninterrupted data (Xue *et al.* 2013; Serrat-Capdevila *et al.* 2014; Ren *et al.* 2018). The SPPs are used in many applications such as weather prediction, agriculture monitoring, and hydrological models (Bitew & Gebremichael 2011; Belabid *et al.* 2019; Dandridge *et al.* 2019; Jamro *et al.* 2019; Dars *et al.* 2020; Krisnayanti *et al.* 2021) such as Soil and Water Assessment Tool (SWAT) (Rathinasamy *et al.*, 2014; Tuo *et al.* 2016; Le *et al.* 2020; Wang *et al.* 2020), Variable Infiltration Capacity (VIC) (Xie & Xiong 2011; Shah & Mishra 2016; Beria *et al.* 2017; Shayeghi *et al.* 2020), Grid-Xinanjiang model (GXAJ) (Yuan *et al.* 2019), Rainfall-Runoff-Inundation (RRI) (Tam *et al.* 2019), and Coupled Routing and Excess Storage (CREST) (Tang *et al.* 2019).

Many studies evaluated the performance of precipitation products at a large basin scale (Saha *et al.* 2010; Fuka *et al.* 2014; Zhang *et al.* 2021). For instance, Tang *et al.* (2019) evaluated the four SPPs using the SWAT model. They found that the Multi-Source Weighted-Ensemble Precipitation (MSWEP) performed relatively better than the other products in the Mekong River Basin in South-East Asia. Try *et al.* (2020) concluded that Tropical Rainfall Measuring Mission (TRMM), Asian Precipitation – Highly-Resolved Observational Data Integration Towards Evaluation (APHRODITE), and Global Precipitation Climatology Centre (GPCC) datasets were suitable for rainfall-runoff and flood inundation modeling at the same basin. Dhanesh *et al.* (2020) evaluated Climate Hazards Group InfraRed Rainfall with Station (CHIRPS) and Climate Forecast System Reanalysis (CFSR) using the SWAT model and found that CHIRPS outperformed CFSR at several basins with different climatic zones. However, only a few studies investigate the performance of precipitation products at a local or regional scale (Bitew & Gebremichael 2011; Yuan *et al.* 2017). This highlights the need to investigate the applicability of various gridded data to such basins.

In the Indian scenario, the different SPPs were evaluated for their accuracy and uncertainty by comparing them with Indian Meteorological Department (IMD) gridded data (Sunilkumar *et al.* 2015; Shah & Mishra 2016; Beria *et al.* 2017; Himanshu *et al.* 2018; Prakash *et al.* 2018; Shukla *et al.* 2019; Thakur *et al.* 2020; Yeggina *et al.* 2020). For instance, Sunilkumar *et al.* (2015) reported on the evaluation and intercomparison of the different SPPs (TRMM-3B42, PERSIANN, CMORPH) that Precipitation Estimation from Remotely Sensed Information using Artificial Neural Networks (PERSIANN) and Climate Prediction Center MORPHing method (CMORPH) severely underestimated the northeast monsoon. The performance of TRMM3B42 was found to be relatively better than the others. However, Yeggina *et al.* (2020) found that TRMM-3B42V7 notably overestimates the light precipitation and underestimates extreme precipitation over a small river basin in southern India. Similarly, during the hydrological evaluation of TRMM-3B42V7 using the SWAT model over a small catchment in southwestern India, Himanshu *et al.* (2018) found that the product underestimated the heavy rainfall amount and showed limited skill on a daily scale and fairly good prediction on a monthly scale. Shukla *et al.* (2019) revealed that TRMM-3B42V7 is limited in capturing rainfall during the monsoon season over the Himalayan region. However, applying bias correction resulted in satisfactory improvement. Due to significant errors in the product over the Himalayan region, Bharti & Singh (2015), Himanshu *et al.* (2018), and Shukla *et al.* (2019) recommended using bias correction methods and improving the retrieval algorithms. Prakash *et al.* (2018) compared TRMM, Integrated Multi-satellite Retrievals for Global

precipitation measurement (IMERG), and Global Satellite Mapping of Precipitation (GSMaP) during the monsoon of 2014 and reported that both IMERG and GSMaP showed improvement over TRMM Multi-satellite Precipitation Analysis (TMPA) in the estimation of low to moderate rainfall distribution across the country. However, the results were preliminary observations solely based on the monsoon season of 2014. Hence, further studies on additional monsoon season were recommended. Most of these studies have focused on quantitative evaluation, and less work has been reported on these products' ability to drive hydrological models.

Therefore, it will be of great interest to the hydrologic community to understand the accuracy of data and its ability to drive hydrological models. Further, it will be helpful to investigate the performance of these precipitations in capturing extreme events in a cyclone-prone region.

This study evaluates three satellite precipitation products (GPM-IMERG, TRMM3B42, and PERSIANN-CDR) over the Vamsadhara River Basin (VRB). The basin is in a tropical climatic regime with semi-arid and semi-humid characteristics. The mainstream originates in the Kalahandi district of Odisha state and flows through approximately 254 km before joining the Bay of Bengal at Kalingapatnam, Andhra Pradesh. Due to the monsoonal winds from the Bay of Bengal branch, the basin often experiences various cyclones during the monsoon season. The specific objectives of the study are:

(i) To evaluate three satellite precipitation products for viz. TRMM-3B42V7, IMERG-GPM V6 (0.1° × 0.1°) and PERSIANN-CDR (0.25° × 0.25°) at different temporal and spatial scales during 2000–2018 at cyclone-prone river basin and
(ii) to assess their ability to drive hydrological models for streamflow simulation at daily and monthly time scales.

The rest of the manuscript has the following structure. **Section 2** describes the data and methods applied in the study, and the results from the study are presented in **Section 3**. The discussion based on the analysis of the results and concluding remarks are provided in **Sections 4 and 5**, respectively.

2. MATERIALS AND METHODS

2.1. Study area

This study has considered Vamsadhara River Basin (VRB) (Figure 1) for evaluating the latest precipitation products. VRB is located between the Godavari and Mahanadi major river basins in Southeast India. It lies between 18°15′N to 20°0′N latitude and 84° 15′E to 84°30′E longitude. The geographical area of the basin is about 10,448 km^2. The study area falls under tropical climatic regions with semi-arid and semi-humid characteristics. The mainstream originates in the Kalahandi district of Odisha state and flows through approximately 254 km before joining the Bay of Bengal at Kalingapatnam, Andhra Pradesh. A significant proportion of the basin area, 78%, comes under forest cover. For more details, the digital elevation map and land use land cover map of the basin are shown in Figure 2.

VRB received an annual rainfall of 1,281 mm during 2000–2018 (Yeditha *et al.* 2020), and most of the rainfall is covered during the southwest monsoon months of June to September. The Indian summer monsoon has two branches from the high-pressure regions of the Arabian Sea and the Bay of Bengal. Due to the monsoonal winds from the Bay of Bengal branch, the basin often experiences various cyclones during the monsoon season. This often invokes various socio-economic losses. For instance, the highly severe tropical cyclonic storm 'Fani' recently hit the state of Odisha in 2019. This was the strongest cyclone after the 1999 Odisha cyclone.

Similarly, the region was hit by the 'HUD HUD' cyclone in 2015. As for the soil characteristics of the basin, around 94% of the basin is covered by sandy clay loam soil.

2.2. Datasets description

In this study, three satellite precipitation products (SPPs), namely, 1) GPM-IMERGV6 data, 2) TRMM 3B42 data, and 3) PERSIANN-CDR data, are used for evaluation. The gauge-based IMD gridded dataset is used as a benchmark for evaluating these SPPs. Detailed information about the precipitation data products is shown in Table 1.

2.2.1. GPM-IMERG data

The Global Precipitation Measurement (GPM) project was developed by the combined effort of the Japan Aerospace Exploration Agency (JAXA) and the National Aeronautics and Space Administration (NASA) of the United States. GPM is a widely used precipitation product throughout the world, and it is also an updated precipitation product of the TRMM. GPM has two primary sensors: one is GPM Microwave Imager (GMI), which helps measure precipitation droplet size, type, and intensity;

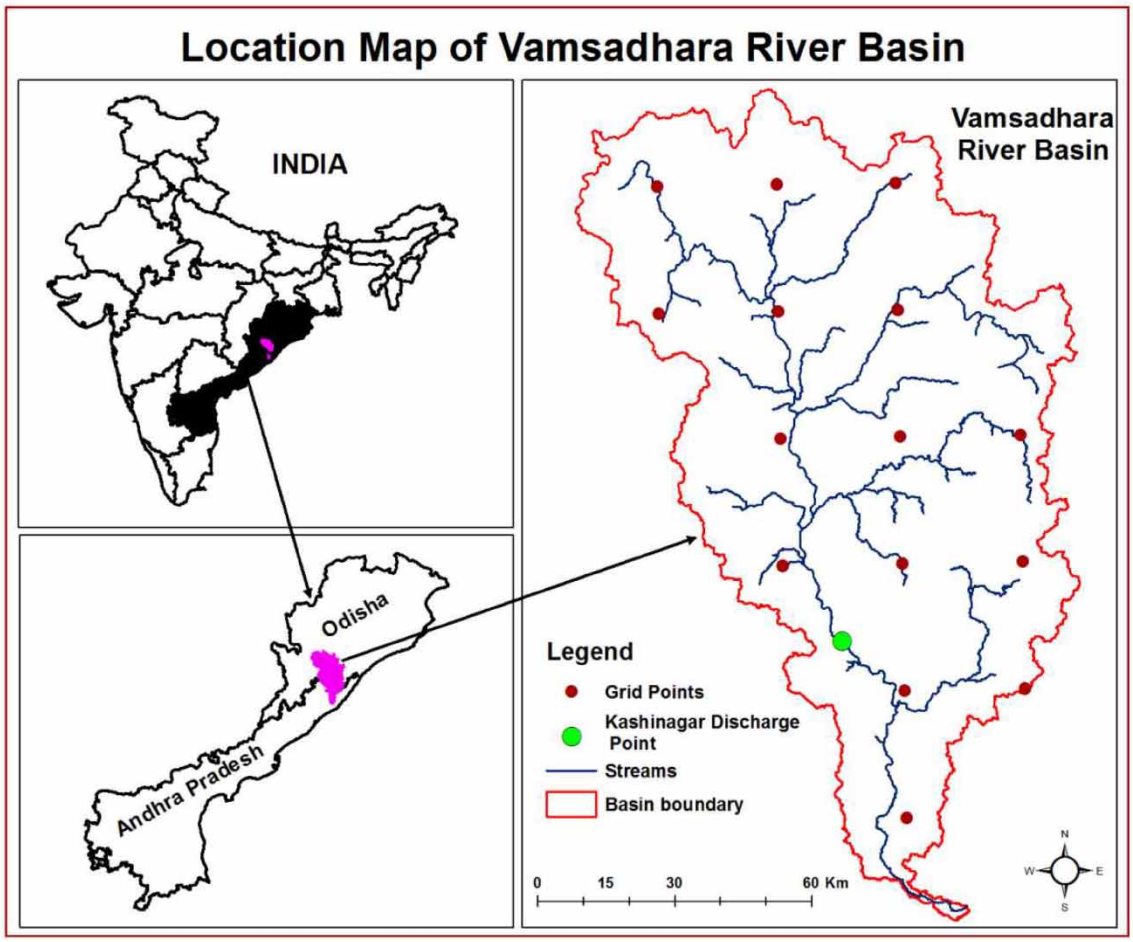

Figure 1 | Map of the Vamsadhara River Basin. The red-colored dots represent the Indian Meteorological Department (IMD) precipitation grid centre locations. The blue lines represent the streams and the green colored circle represents the location of the river gauge discharge monitoring point at Kashinagar. The discharge data at this gauging station was used for the SWAT model calibration.

the second one is a Dual-frequency Precipitation Radar (DPR), which measures the internal structure of clouds (Hou *et al.* 2014). The GPM microwave imager has more frequency channels than TRMM, and the precipitation radar is more advanced (Hou *et al.* 2014). More importantly, spatial coverage (60° S–60° N) and the spatiotemporal resolution (30 min and (0.1° × 0.1°)) have been improved compared to the previous SPPs.

The GPM team has developed GPM-IMERG precipitation products. The IMERG algorithm first calibrated the microwave precipitation estimates (derived from the constellation of the microwave satellite sensors) using the Global Precipitation Climatology Project (GPCP) monthly estimates to reduce bias. The algorithm uses the Climate Prediction Centre Morphing-Kalman Filter (CMORPH-KF) quasi-Lagrangian time interpolation to estimate finer time and space scales. The CMORPH-KF quasi-Lagrangian interpolation uses both the inter-calibrated microwave estimates and the PERSIANN-CCS estimates (Infra-Red estimates) to generate precipitation estimates at half-hourly temporal resolution. Currently, three IMERG products are available: early run, late run, and final run, with a latency period of 4 h, 14 h, and 3.5 months, respectively. The first two products are helpful in real-time application, whereas the latter can be used for water balance studies. All these products are available at 0.1° × 0.1° spatial resolution over the fully global domain.

Presently, IMERG is at its Version 06 stage (https://gpm.nasa.gov/missions/two-decades-imerg-resources). A new aspect of the data processing in Version 06 IMERG is that the algorithm combines the data collected during the TRMM era (2000–2014) with the precipitation estimates collected during the GPM era. Due to this, IMERG has now been available since June 2000 (https://gpm.nasa.gov/data/directory). The 'Final run' of IMERG combines the GPCC Monitoring product, the V8 Full Data Analysis, for most of the time (currently 2000–2019).

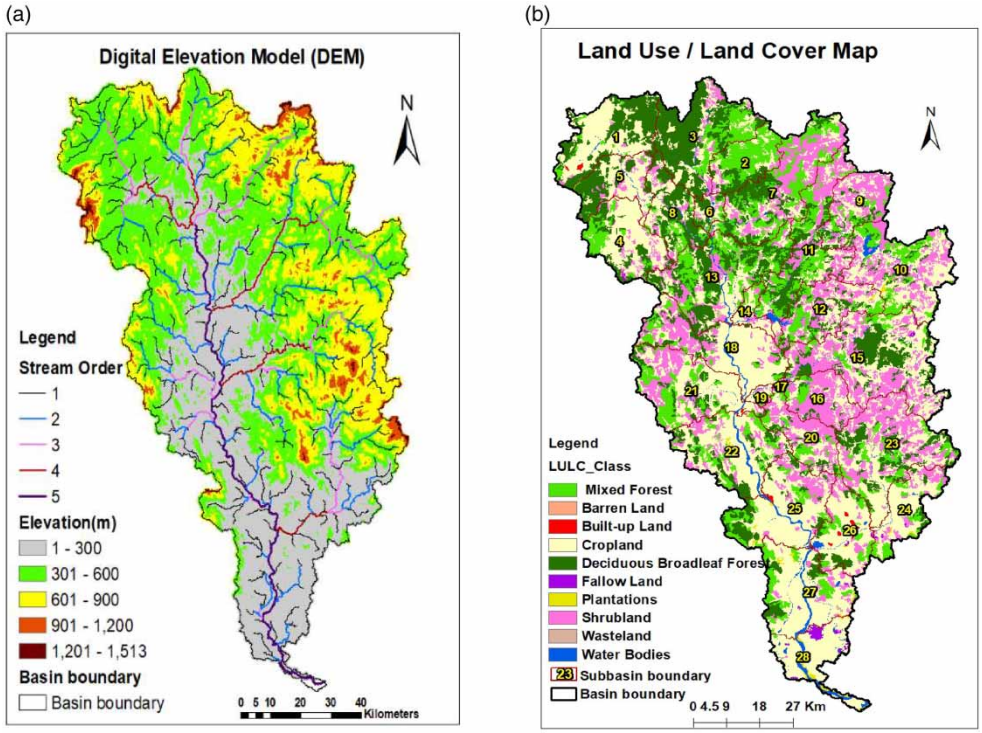

Figure 2 | Map showing the elevation and land use land cover for the Vamsadhara River Basin. (a) is the elevation map prepared from Shuttle Radar Topography Mission (SRTM) Digital Elevation Model (DEM). The drainage lines are also presented in the map, (b) is land use land cover map prepared from the Global Irrigated Area Mapping (GIAM) product developed by the International Water Management Institute (IWMI).

Table 1 | Details of precipitation products with spatial/temporal resolutions and their source

Dataset	Long Name	Coverage	Period	Spatial Resolution	Temporal Resolution	DOI	Data Source
IMD	Indian Meteorological Department	20°N–78° E	1901–2018	0.25°	Daily	–	https://imdpune.gov.in/Clim_Pred_LRF_New/Grided_Data_Download.html
TRMM-3B42	TRMM (TMPA) Precipitation L3 1 day 0.25 degree × 0.25 degree V7	50°S-N	1998-present	0.25°	Daily	10.5067/TRMM/TMPA/DAY/7	https://disc.gsfc.nasa.gov/datasets/TRMM_3B42_Daily_7/summary
PERSIANN-CDR	Precipitation Estimation from Remotely Sensed Information using Artificial Neural Networks- Climate Data Record	60°S-N	1983-present	0.25°	Daily	10.1175/BAMS-D-13-00068.1	https://chrsdata.eng.uci.edu/#tabPERSIANNCDR
GPM-IMERG	GPM IMERG Final Precipitation L3 1 day 0.1 degree × 0.1 degree V06 (GPM_3IMERGDF)	60∘S-N	2000-present	0.1°	Daily	10.5067/GPM/IMERGDF/DAY/06	https://disc.gsfc.nasa.gov/datasets/GPM_3IMERGDF_06/summary?keywords=%22IMERG%20final%22

2.2.2. TRMM data

The Tropical Rainfall Measuring Mission (TRMM) is a joint mission developed by the Japan Aerospace Exploration Agency (JAXA) and the National Aeronautics and Space Administration (NASA) to measure tropical precipitation. The TRMM Multi-Satellite Precipitation Analysis (TMPA) product is obtained from the combination of multi-satellite (microwave and infrared satellites) and GPCC monthly gauge precipitation, and more details are available about TMPA in Huffman *et al.* (2007). TRMM 3B42 version 7 (TRMM-3B42V7) is one type of TMPA product, and it covers a latitude from 50°N to 50°S with a resolution of 0.25° from 1997 to 2018. The TRMM 3B42 daily precipitation data were obtained from this website https://disc.gsfc.nasa.gov/datasets/TRMM_3B42_Daily_7/summary.

2.2.3. PERSIANN-CDR data

PERSIANN-CDR is retrospective satellite precipitation data developed by the National Oceanic and Atmospheric Administration (NOAA) which is widely used to study climatology and hydrological studies (Ashouri *et al.* 2015). The PERSIANN-CDR algorithm is used for generating rain rates from satellite imagery using an artificial neural network (ANN) model, which entirely depends on the combination of Infrared (IR) and Passive Microwave (PMW) observations developed by geostationary and low earth orbit satellites, respectively (Nguyen *et al.* 2018). This product has been available daily from 1983 to the present, covering between 60° S and 60° N with 0.25° resolution. PERSIANN-CDR products have been downloaded from this website https://chrsdata.eng.uci.edu/#tabPERSIANNCDR, and for more details on the PERSIANN-CDR product, the readers can refer to Ashouri *et al.* (2015) and Nguyen *et al.* (2018).

2.2.4. IMD data

In the present study, the IMD gridded data (IMD 4) having a spatial resolution of 0.25° × 0.25° has been used as ground validation. The temporal resolution of the data set is daily. The data sets were developed based on the rainfall records from 6,955 rain gauges across the country (Pai *et al.* 2014). Around 30 rain gauges fall within the study region considered. These rain gauges were partly maintained by IMD, Agromet Department, and mainly by the State Government. Using the Shepard Interpolation method, the collected rainfall from the rain gauges has been converted into the gridded data set. For detailed information, the readers can refer to Pai *et al.* (2014). The data set is available from 1901 to the present; however, for this study, the data set for 2000–2018 is considered. The datasets can be obtained from the Indian Meteorological Department, Pune, https://imdpune.gov.in/Clim_Pred_LRF_New/Grided_Data_Download.html. Several studies confirm the reliability of the IMD gridded dataset (Venkata Rao *et al.* 2020; Yeggina *et al.* 2020). Hence, the IMD gridded data is used as a benchmark for comparing the three satellite precipitation products.

The spatial resolution of the satellite precipitation products, TRMM, and PERSIANN, was 0.25 degrees, the same as the IMD dataset. However, the IMERG dataset has a higher spatial resolution of 0.1 deg. The IMERG data was sampled at the grid locations of the IMD data by using bilinear interpolation to have the same spatial resolution for comparison.

2.2.5. Other data sets for hydrological modelling

The hydrological model requires both spatial and temporal data as input. The temporal data are meteorological (such as temperature, solar radiation, relative humidity, and wind speed) and hydrological observation data (discharge). The meteorological data were collected from the Climate Forecast System Reanalysis (CFSR) reanalysis product. These data were downloaded from https://globalweather.tamu.edu/. The daily discharge data at the Kasinagar gauging station was downloaded from https://indiawris.gov.in/wris/. The spatial information includes the digital elevation model, land use and cover, and soil characteristics. Table 2 describes the spatial, weather, and discharge input data used in developing the SWAT model.

2.3. Evaluation methods for precipitation products

Statistical analysis is used to evaluate satellite precipitation products with reference precipitation data. For this study, we have used (i) continuous statistical metrics (Correlation Coefficient (CC), Root Mean Square Error (RMSE), Mean Absolute Error (MAE), Percentage Bias (PB), Standard Deviation (SD)), (ii) categorical statistical metrics (Probability of Detection (POD), False Alarm Ratio (FAR), Critical Success Index (CSI)), and (iii) empirical distribution function and (iv) hydrological model-based investigation for evaluating the different precipitation products such as TRMM-3B42V7, GPM-IMERGV6, PERSIANN-CDR with reference of IMD precipitation product throughout 2000–2018. All the evaluations were done at different temporal scales (daily, monthly, seasonal, and yearly) and spatial (at grid and basin-scale) scales.

Table 2 | Data sources and description for the spatial, meteorological and hydrological inputs for the SWAT model

Data type	Scale/year	Source
DEM	30 m × 30 m (2014)	Shuttle Radar Topography Mission (SRTM) of USGS (https://earthexplorer.usgs.gov/)
LULC	500 m (2000)	GIAM-IWMI (http://waterdata.iwmi.org/applications/giam2000/giam.php)
Soil	1:1,500,000 (2003)	Food and Agriculture Organization (FAO) http://www.fao.org/soils-portal/soil-survey/soil-maps-and-databases/en/
Temperature	1° × 1°; Daily (1969–2018)	Indian Metrological Department (IMD), http://www.imdpune.gov.in/
Solar Radiation, Relative Humidity, Wind Speed	0.31°; Daily (1979–2014)	Climate Forecasting System Reanalysis (CFSR) https://globalweather.tamu.edu
River Discharge	Point data at Khasinagar; Daily (2000–2012)	Central Water Commission (CWC) (www.india-wris.nrsc.gov.in/)

2.3.1. Categorical analysis

The categorical statistical metrics such as Probability of Detection (POD), False Alarm Ratio (FAR), and Critical Success Index (CSI) have been used for the detection of precipitation capability of satellite precipitation products with reference precipitation products depending on rainy and non-rainy days. POD represents the hit rate, which means the ratio of correctly detected by satellite as a rainfall event to the actual total rainfall events measured by reference data. It varies from 0 to 1 (1 is the ideal value). FAR is known as a false rate. It represents the ratio of satellite-detected falsely as a rainfall event to the total rainfall events detected by satellite. It varies from 0 to 1 (0 is the perfect value). CSI is the ratio of correctly detected rainfall events by satellite to the total number of hits, misses, and false alarms. CSI values range from 0 to 1 (1 is a suitable value), as shown in Table 3.

Apart from the metrics discussed above, the empirical distribution is a handy feature for evaluating the distribution of the total rainfall into different precipitation intensity categories. As per World Meteorological Organization (WMO) standard Geneva, 2012, daily rainfall is divided into seven classes based on rainfall intensity, namely 0–1 mm/day, 1–2 mm/day, 2–5 mm/day, 5–10 mm/day (high moderate rain), 10–20 mm/day (low heavy rain), 20–50 mm/day (high heavy rain), >50 mm/day (extreme rain) Setti *et al.* (2020a, 2020b).

2.3.2. Continuous statistical metrics

To evaluate SPPs quantitatively, we have used statistical accuracy indicators such as CC, SD, MAE, Pbias, and RMSE. CC described the degree of linear correlation between the satellite and observed precipitation products, ranging from −1 to 1, representing perfect correlation, either negative or positive correlation, respectively (CC value 0 represents no correlation). The RMSE, MAE, and Pbias measure the error and bias of satellite precipitation products with reference precipitation products, respectively (see Table 3). When the RMSE value is smaller, the SPPs data are close to the observed precipitation data. Pbias has positive and negative values representing the underestimation and overestimation by the SPPs, respectively.

2.4. Hydrologic model-based evaluation

In this study, the Soil Water Assessment Tool (SWAT) model was used for the hydrologic model-based evaluation of the precipitation products. The satellite precipitation products were used as input precipitation for a calibrated model, and the streamflow simulation was compared at different time scales. Details about the SWAT model are provided in section 2.4.1. To evaluate the effect of four precipitation products on streamflow, two scenarios were generated: Scenario A and Scenario B. In scenario A, first, the model was calibrated with IMD precipitation data; then, the same model was run with other precipitation products such as GPM-IMERGV6, TRMM-3B42V7, and PERSIANN-CDR. For this purpose, first, the SWAT model was developed with IMD data; after calibration and validation, the model was driven using other precipitation products for the validation period. In scenario B, individual models were calibrated and validated for each precipitation product. The results of scenario B are discussed in the supplementary material.

Based on data availability, such as observed streamflow data and precipitation products, the total period is divided into three parts: warm-up period (2000–2001), calibration period (2002–2010), and validation period (2011–2016). Additionally,

Table 3 | Details of the continuous and categorical statistical metrics used for evaluating the precipitation products

Statistic Metric	Equation	Perfect Value	Description
Nash-Sutcliffe Coefficient Efficiency (NSE)	$NSE = 1 - \left[\frac{\sum_{i=1}^{n}(Y_i^{obs} - Y_i^{sim})^2}{\sum_{i=1}^{n}(Y_i^{obs} - Y_{mean}^{obs})^2}\right]$	1	It measures the model performance
Correlation Coefficient (CC)	$CC = \frac{\sum_{i=1}^{n}(Y_i^{sim} - Y_{mean}^{sim})(Y_i^{obs} - Y_{mean}^{obs})}{\sqrt{\sum_{i=1}^{n}(Y_i^{obs} - Y_{mean}^{obs})^2}\sqrt{\sum_{i=1}^{n}(Y_i^{sim} - Y_{mean}^{sim})^2}}$	1	It represents the degree of agreement in between observed and measured data
Root Mean Square Error (RMSE)	$RMSE = \frac{\sqrt{\sum_{i=1}^{n}(Y_i^{obs} - Y_i^{sim})^2}}{N}$	0	It represents the magnitude of average error
Percent Bias (Pbias)	$Pbias = \frac{\sum_{i=1}^{n}(Y_i^{obs} - Y_i^{sim}) \times 100}{\sum_{i=1}^{n}(Y_i^{obs})}$	0	It represents the deviation between observed and measured data
Mean Absolute Error (MAE)	$MAE = \frac{1}{n}\sum_{i=1}^{n}\lvert Y_i^{sim} - Y_i^{obs}\rvert$	0	It measures the average difference in between observed and estimated data
Probability of Detection (POD)	$POD = H/(H + M)$	1	It represents the detected rainfall events correctly by satellite out of rainfall events by reference data.
False Alarm Ratio (FAR)	$FAR = F/(F + H)$	0	It represents the false, detected rainfall event by satellite when reference data showed no rainfall
Critical Success Index (CSI)	$CSI = H/(H + M + F)$	1	It shows more accuracy when correct negative values are not considered

the models were calibrated and validated at daily and monthly time scales using the daily observed streamflow and mean monthly streamflow for both scenarios.

2.4.1. SWAT model

The Agriculture Research Service of the United States Department of Agriculture developed the SWAT model. The SWAT model can be used for predicting the different hydrological components like erosion, water balance, vegetation growth, evapotranspiration, and water quality of watersheds by solving processes based on the water balance equation in daily time steps. The surface runoff is estimated by using the Soil Conservation Service (SCS) -Curve Number (CN) method. The SWAT model is simulated percolation using the storage routing technique, which assumes that percolation occurs when the water content exceeds the field capacity and the layer below is unsaturated (Abbaspour *et al.* 2015). Also, the SWAT model has three methods for estimating Potential Evapotranspiration (PET). These are Priestley Taylor (Priestley & Taylor, 1972), Hargreaves (Hargreaves & Samani 1985), and Penman-Monteith (Monteith, 1965). In this study, the Penman-Monteith method is used for estimating potential evapotranspiration. SWAT divides the whole basin into sub-basins and Hydrological Response Units (HRUs) based on the unique land use, soil, and slope combination (Setti *et al.* 2018).

2.4.2. Model setup

The QSWAT (version 1.3) tool used to develop the Vamsadhara River Basin model interfaced with QGIS 2.6.1. All spatial input data was re-projected and resampled to 30 m spatial resolution for the SWAT model. The generation of stream network and delineation of watersheds was done using the TauDEM tool in QSWAT. The entire study area was divided into 26 sub-basins using a threshold of 150 km^2 then subdivided into 543 Hydrological Response Units (HRUs). The HRUs are the smallest component in the SWAT model and are unique land use, soil, and slope combinations. The sensitivity analysis,

auto-calibration, and validation were done by using SWAT CUP 2012 software with the SUFI-2 algorithm (please refer to Abbaspour *et al.* (2007) and Setti *et al.* (2020a, 2020b) for more details). Numerous iterations, with 2000 simulations, were run for model calibration of the IMD precipitation product using SWAT CUP. This study adopts a global sensitivity method for sensitivity analysis (Abbaspour *et al.* 2007).

Several error measures are available to evaluate the performance of the hydrological model in simulating streamflow (Guo & Su 2019). In this study, we have adopted the Correlation Coefficient (CC), Nash–Sutcliffe coefficient (NS) (Nash & Sutcliffe, 1970), and Percent Bias (Pbias) for performance analysis. The mathematical formulations are provided in Table 3. NS represents the quantity difference between observed and simulated streamflow and ranges from -∞ to 1 (1 is the ideal value). Pbias values provide the percentage of bias involved in the streamflow estimates. If Pbias is positive (negative), the model underestimates (overestimates) the streamflow concerning the observed data. The methodology flow chart used in the study is shown in Figure 3.

3. RESULTS

3.1. Evaluation at the daily scale

In this study, we evaluated the three satellite precipitation products (TRMM-3B42V7, GPM-IMERGV6, PERSIANN-CDR) compared to IMD gridded precipitation products using statistical metrics such as CC RMSE, MAE, RB, and SD, as shown in Table 4. As per statistical metrics of all precipitation products at a daily time scale, GPM-IMERGV6 has a better correlation value (0.48) compared to TRMM-3B42V7 (0.44) and PERSIANN-CDR (0.36) precipitation products. The GPM-IMERGV6 product has the lowest error value in terms of RMSE (9.5 mm/d) and MAE (3.8 mm/d) compared to TRMM-3B42V7 and PERSIANN-CDR data. Thus, based on statistical metrics, GPM-IMERGV6 is close to the IMD precipitation product. PERSIANN-CDR data show inferior performance compared to the TRMM-3B42V7 and GPM-IMERGV6. The three satellite products (TRMM-3B42V7, IMERGV6, PERSIANN-CDR) seem to overestimate precipitation amount compared to IMD precipitation amount for the period of 2000–2018 as the negative percentage bias (%) range from 3.8% (GPM-IMERGV6) to 22.4% (PERSIANN-CDR). The standard deviation was low (9 mm) for TRMM-3B42V7 and was 9.5 and 12 mm for GPM-IMERGV6 and PERSIANN satellite precipitation products. Overall, the IMERGV6 and PERSIANN-CDR products showed the best and worst performance, respectively, based on five statistical metrics, as shown in Table 4.

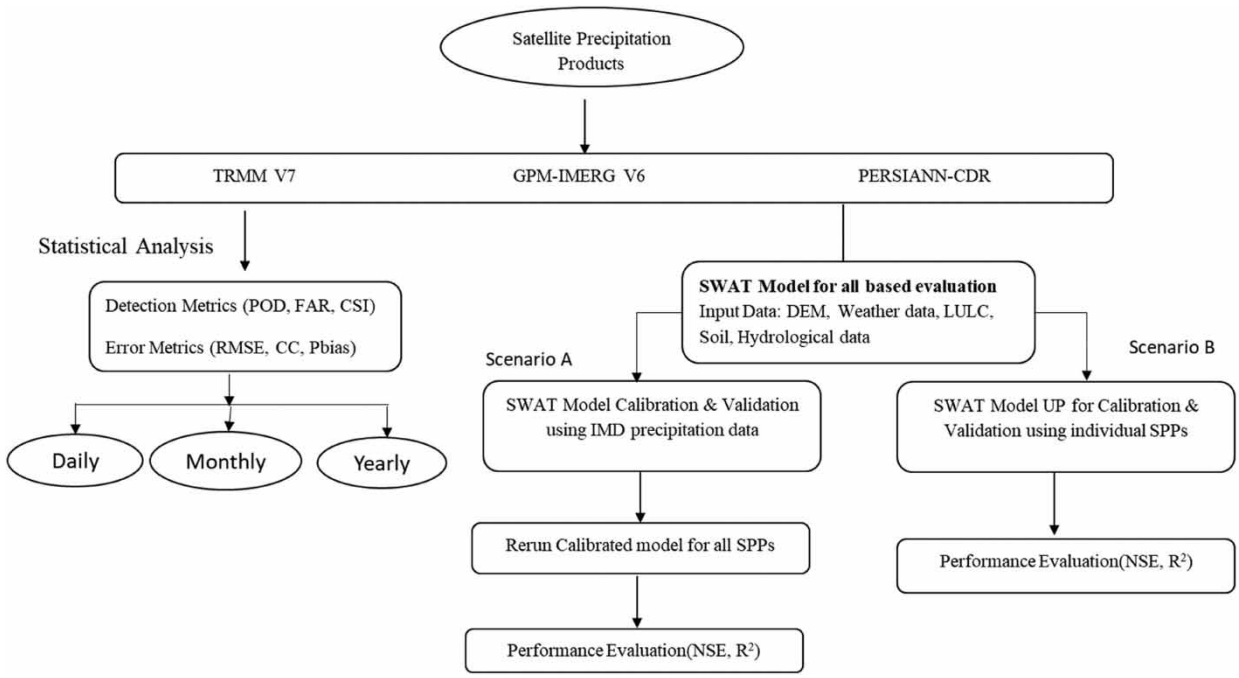

Figure 3 | Flowchart for the methodology used in the present study.

Table 4 | Comparison of continuous statistical metrics of all precipitation products at daily, monthly, and yearly time scale at watershed scale

	Daily			Monthly			Yearly		
Statistical Indicator	**TRMM**	**GPM**	**PERSIANN**	**TRMM**	**GPM**	**PERSIANN**	**TRMM**	**GPM**	**PERSIANN**
Correlation	0.44	0.48	0.36	0.94	0.93	0.78	0.62	0.62	0.23
RMSE	9.58	9.52	12.35	41.60	43.16	63.61	212.67	182.46	256.24
MAE	3.97	3.84	5.39	26.75	27.86	36.93	169.99	160.00	278.89
SD	9.0	9.5	12.0	121.6	117.4	167.9	187.0	168.6	204.1
Percent Bias (%)	−8.7	−3.8	−52.4	−8.7	−3.8	−52.4	−8.7	−3.8	−52.4

3.1.1. Grid-wise analysis

Figure 4 shows the spatial distribution of the CC and RMSE for the three SPPs. For a direct comparison of the precipitation products with the same scale, please refer to the supporting document Figure S1. All the products show a good correlation in the northwestern part of the study area but have a low correlation in the southern part. GPM-IMERGV6 shows a better correlation value of 0.48 (average value of 15 grids) than the TRMM-3B42V7 (0.44) and PERSIANN-CDR (0.36) and the lowest RMSE value of 9.52 mm/day than the TRMM-3B42V7 (9.58 mm/day) and PERSIANN-CDR (12.35 mm/day) as shown in Table 4. GPM-IMERGV6 and PERSIANN-CDR products show an increasing RMSE trend from west to east in the study area and while the TRMM-3B42V7 product shows an increasing trend from south to north in the study area, as shown in

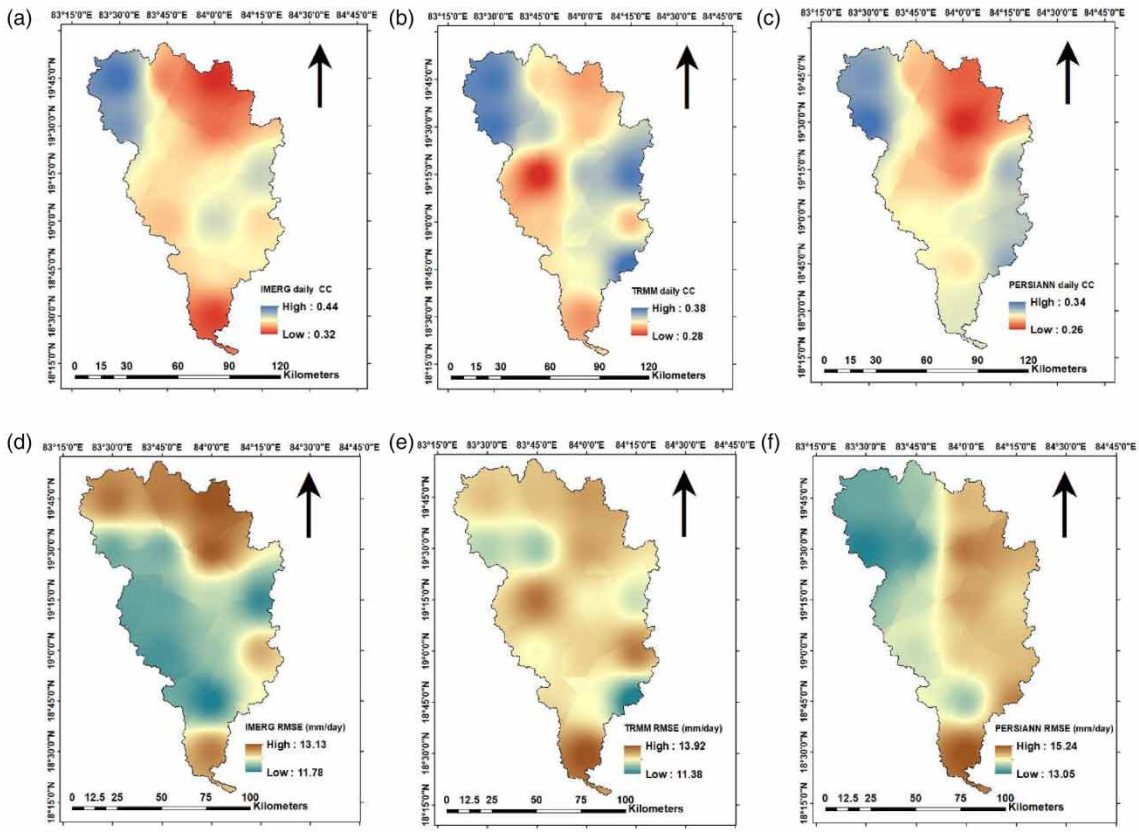

Figure 4 | The spatial distribution of correlation coefficient of (a) IMERG (b) TRMM (c) PERSIANN; root mean square error of (d) IMERG (e) TRMM (f) PERSIANN at daily scale over the period 2000–2018. The spatial maps were created from the statistical metrics at 15 grid points using Inverse Distance Weighted interpolation (IDW) in ArcMap.

Figure 4. Compared to all precipitation products, the GPM-IMERGV6 product shows better correlation and lower error values compared with TRMM-3B42V7 and PERSIANN-CDR data sets at a daily scale.

Table 5 presents the distribution of the rainfall events in terms of the rainfall intensity classifications. Among the seven classes, the very light rain (0 to 1 mm/d) class has the highest probability, and the extreme rain (>50 mm/d) class has the lowest probability in both the SPPs and gridded precipitation product.

3.1.1.1. Very light rain. It is observed that the GPM-IMERGV6 and TRMM-3B42V7 have frequent very light rain indicating a high false alarm rate. However, the PERSIANN-CDR (943 days) have a more or less similar number of rainy days with the IMD (930 days) (see Table 6). The IMD receives 1.6% of the total rainfall in terms of precipitation amount, while the GPM, TRMM-3B42V7, and PERSIANN-CDR receive 2.8, 2.1, and 1%, respectively.

3.1.1.2. Light rain and low moderate rain. In this rainfall category, the GPM and TRMM-3B42V7-based estimates are close to IMD regarding the number of rainfall days and the amount of precipitation. However, PERSIANN-CDR data has fewer rainy days and underestimates the magnitude of light rain and low, moderate events.

3.1.1.3. High moderate rain. 16.8% (IMD) of the total precipitation falls in this rainfall category. For the GPM, TRMM-3B42V7 and PERSIANN-CDR, 16.9%, 16.7%, and 9.9% fall in this category, respectively. This indicates that the GPM and TRMM-3B42V7 could capture the magnitude of rainfall in this category. However, the PERSIANN-CDR receives noticeably less rainfall.

Table 5 | Probability of occurrence precipitation and their rainfall quantity percentage for comparison of precipitation products (IMD, TRMM, GPM-IMERG, and PERSIANN) based on World Meteorological Organization standards during the period of 2000–2018

		Number of Days				Precipitation quantity (%)			
Rainfall category (mm)		IMD	TRMM	GPM	PERSIANN	IMD	TRMM	GPM	PERSIANN
Dry days	0	3,519	1,226	3,067	3,356	0	0	0	0
Very light rain	0 to 1	930	3,094	1,346	943	1.6	2.8	2.1	1.0
Light rain	1 to 2	447	471	478	352	2.7	2.7	2.8	1.4
Low moderate rain	2 to 5	726	709	714	576	9.7	8.9	9.5	5.2
High moderate rain	5 to 10	571	615	592	514	16.8	16.9	16.7	9.9
Low heavy rain	10 to 20	472	514	446	584	26.9	26.8	24.7	22.3
High heavy rain	20 to 50	230	268	250	516	27.9	29.9	29.4	41.3
Extreme rain	>50	45	43	47	99	14.3	12.0	14.9	18.8
Total	–	6,940	6,940	6,940	6,940	100	100	100	100

Table 6 | Comparison of statistical metrics of all precipitation products for spring, summer, fall and winter seasons during 2000 to 2018 at watershed scale

	Spring			Summer			Fall			Winter		
Statistical Indicator	TRMM	GPM	PERSIANN	TRMM	GPM	PERSIANN	TRMM	GPM	PERSIANN	TRMM	GPM	PERSIANN
CC	0.18	0.21	0.16	0.35	0.41	0.29	0.47	0.50	0.41	0.30	0.19	0.03
RMSE	94.68	78.72	154.37	200.74	195.54	256.05	159.39	152.26	158.26	32.30	31.33	28.32
MAE	37.75	33.25	67.72	121.00	113.68	157.37	41.43	40.31	41.30	6.67	6.44	5.20
SD	76.02	52.29	142.75	185.60	193.59	240.81	144.29	137.7	116.89	26.56	20.61	3.89
Percent Bias (%)	−23.96	0.98	−170.73	−16.88	−10.48	−57.42	10.03	14.78	23.19	5.98	29.57	90.76

3.1.1.4. Low heavy rain. Based on the values shown in Table 5, TRMM-3B42V7 (514 days) and GPM-IMERGV6 (446 days) have a slight tendency for false alarms and misses, respectively, concerning the IMD data (472 days). But the estimates for PERSIANN-CDR seem to have a higher tendency for false alarms (584 days). This means that the PERSIANN-CDR has more frequent low heavy rains, contributing to the overall high overestimation of the magnitude of rainfall.

3.1.1.5. High heavy rain and extreme rain. In this category also, the GPM (250 days, 29.4%) and TRMM-3B42V7 (268 days, 29.9%) were close to the IMD (230 days, 27.9%) in terms of the number of rainy days and the percentage (out of the total rainfall depth) of the rainfall received. However, the PERSIANN-CDR (516 days and 41.3%) data-based estimates overestimate the precipitation. A similar pattern was observed for extreme rain, where PERSIANN-CDR data showed significant false alarms and overestimations. This frequent heavy and extreme rainfall resulted in overestimated rainfall at the basin.

The categorical analysis results in detection metrics at different precipitation thresholds of 1–10 mm/day, 10–50 mm/day, and >50 mm/day is shown in Figures 5 and 6. Figure 5 shows that the IMERG V6 has POD values ranging from 0.57 to 0.64. In contrast, the 3B42V7 and PERSIANN-CDR yielded POD values in the range of 0.42–0.72 and 0.60–0.69, respectively, showing that the TRMM and PERSIANN products have better detection capabilities in the light rain category. For moderate rainfall, the IMERG v6 has POD values near 0.40 for most of the basin, whereas the 3B42V7 and PERSIANN showed POD in the range of 0.32–0.41 and 0.39–0.44, respectively. For heavy rainfall events, the performance of IMERGV6 is comparatively better than the 3B42V7 and PERSIANN-CDR in terms of POD. The spatial average of POD over the study area was found to be 0.27, 0.21, and 0.18 for IMERGv6, 3B42V7, and PERSIANN-CDR, respectively. Even though the analysis reveals that the POD decreases with the increasing rainfall intensity, this must be understood with caution based on the detection definition. This study defines a missed rainfall event as an event below the rainfall threshold. Therefore, apart from POD, multiple criteria for assessment, such as RMSE, have been employed in this study period.

For FAR, the performance of the SPPs was more or less similar in the light rainfall category, with the values ranging from 0.37–0.57 (see Figure 6). The FAR was high in the eastern part of the catchment near the ocean. For the moderate rainfall category, the performance of the IMERGV6 is comparatively better than the other two products in terms of the FAR values. The FAR values ranged between 0.62–0.68, 0.65–0.69, and 0.70–0.75 for IMERGV6, 3B42V7, and PERSIANN-CDR, respectively. For the heavy rainfall category, the PERSIANN-CDR data tend to have higher FAR values for most of the study region, indicating a higher tendency for false alarms. The average values for FAR over the study region (Figure 7) show that the FAR between the IMERGV6 and PERSIANN-CDR is significant for the heavy rainfall category. In contrast, there is no considerable difference between IMERGV6 and TRMM-3B42V7.

In the case of average Critical Success Index (CSI) values, as shown in Figure 7, the PERSIANN-CDR data shows a low success rate compared to the TRMM-3B42V7 and GPM-IMERGV6 for all three thresholds.

Overall, from the analysis of the daily scale, it can be summarized that the TRMM-3B42V7 and GPM-IMERG V6 estimates are close to IMD based on the statistical analysis and detection metrics. In contrast, the PERSIANN-CDR estimates seem to overestimate and provide false alarms, particularly during high rainfall days.

3.2. Evaluation at monthly time scale

The correlation (Table 4) between the IMD gridded data and satellite data sets such as TRMM-3B42V7, GPM-IMERGV6, and PERSIANN-CDR products was found to be 0.94, 0.93, and 0.78, respectively. This indicates that the TRMM-3B42V7 and GPM-IMERG V6 data products were better correlated with IMD gridded data than the PERSIANN-CDR data. Regarding average RMSE and MAE, the SPPs have shown significant variation with PERSIANN-CDR data yielding higher values. Other statistics such as Standard Deviation (SD) and percent bias were also higher for PERSIANN-CDR data, indicating overestimated rainfall in the study area. The average monthly rainfall and the monthly MAE associated with these estimates across the entire study area are shown in Figure 8(a) and 8(b), respectively. Figure 8(b) shows that the PERSIANN-CDR product has a high overestimation from May to September. This can be attributed to persistent heavy rains and high false alarms during the monsoon months. Similar results were reported by Tan & Santo (2018).

Comparing the average monthly precipitation for 19 years between IMD gridded and satellite precipitation products, there is a tendency for slight overestimation during monsoon months (June to September) using the GPM-IMERGV6 and TRMM-3B42V7 data. But the PERSIANN product tends to highly overestimate precipitation during monsoon months and

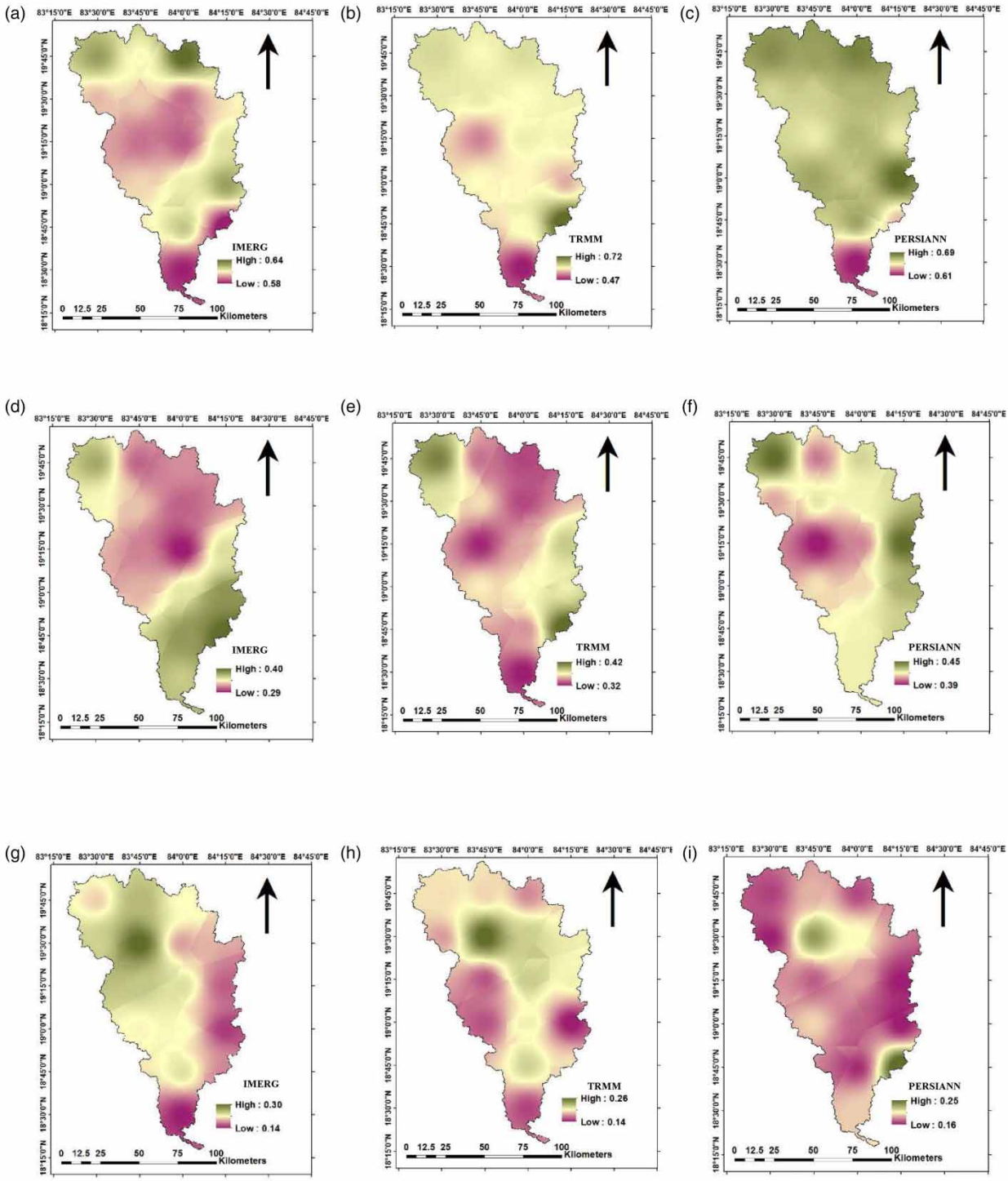

Figure 5 | POD for the different precipitation products at different precipitation intensity thresholds. (a–c) 1mm-10 mm/day threshold, (d–f) 10mm-50 mm/day threshold and (g–i) > 50 mm/day threshold. The columns from the left represent the results from GPM-IMERG V6, TRMM-3B42v7 and PERSIANN-CDR. The spatial maps were created from the statistical metrics at 15 grid points using Inverse Distance Weighted interpolation (IDW) in ArcMap.

underestimate from November to March. Patterns in mean absolute error (MAE) for all satellite precipitation products followed the average monthly precipitation pattern of precipitation products. The higher MAE values occurred in monsoon months when precipitation is high, with lower MAE in summer months when precipitation is low.

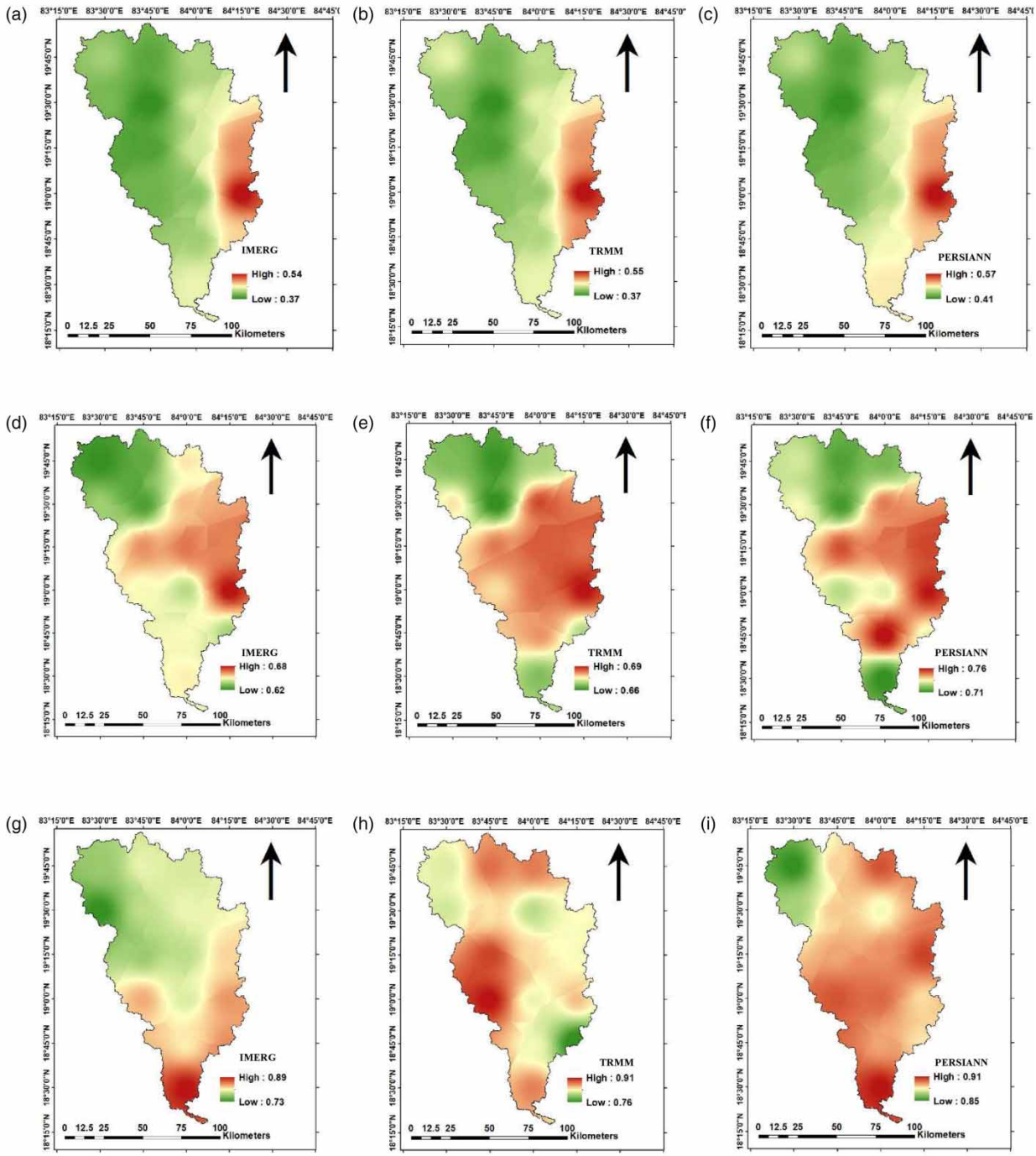

Figure 6 | FAR for the different precipitation products at different precipitation intensity thresholds. (a–c) 1mm-10 mm/day threshold, (d–f) 10 mm-50 mm/day threshold and (g–i) > 50 mm/day threshold. The columns from the left represent the results from GPM-IMERG V6, TRMM-3B42v7 and PERSIANN-CDR. The spatial maps were created from the statistical metrics at 15 grid points using Inverse Distance Weighted interpolation (IDW) in ArcMap.

At the monthly scale, GPM-IMERGV6 and TRMM-3B42V7 precipitation products have nearly similar MAE values, 36 and 38 mm/month, respectively. PERSIANN-CDR has the highest MAE value (83 mm/month). A similar pattern was observed for RMSE and standard deviation. Figure 9 shows the spatial distribution of correlation and RMSE over the period 2000–2018. For a better comparison of the precipitation products with the same color scale, please refer to the supporting

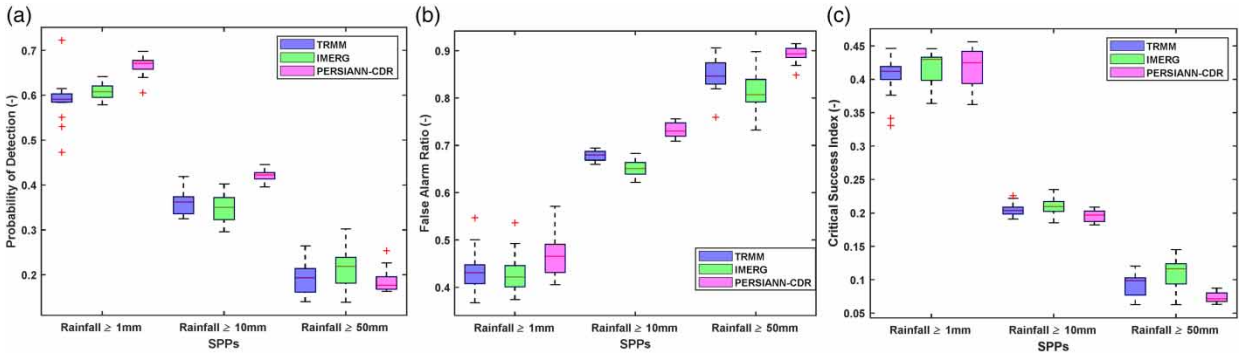

Figure 7 | Results from statistical evaluation of precipitation products (TRMM, GPM-IMERG, and PERSIANN) using metrics: (a) Probability of Detection (POD), (b) False Alarm Ration (FAR), (c) Critical Success Index (CSI).

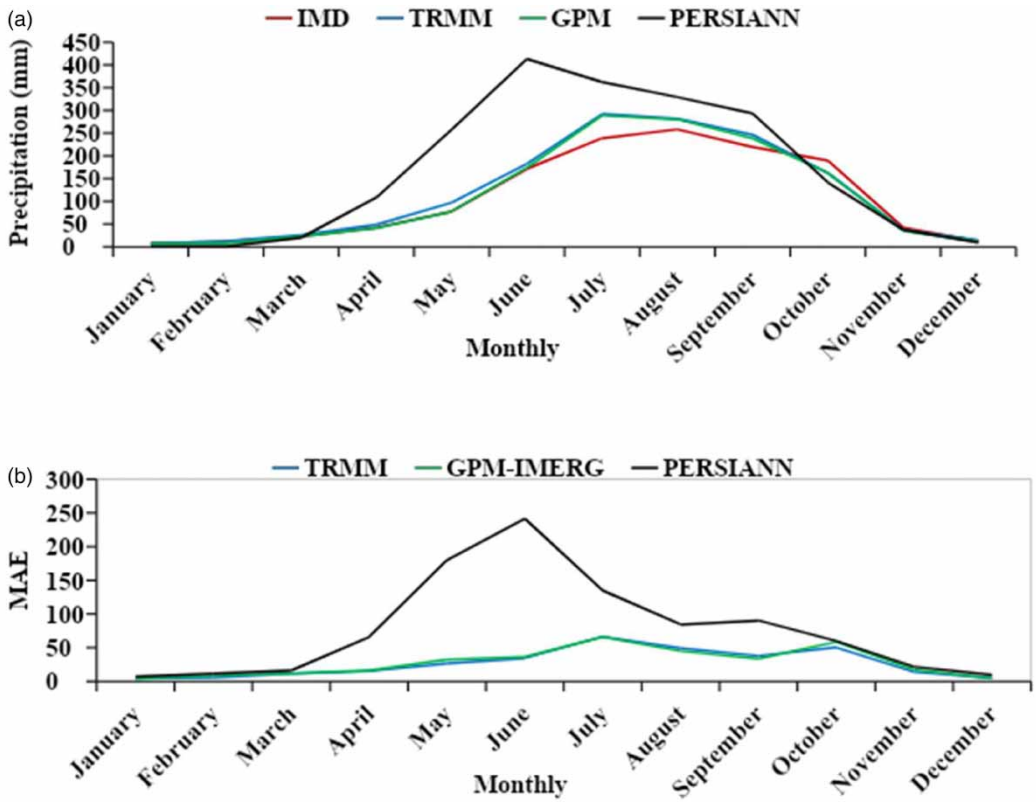

Figure 8 | (a) Average monthly precipitation of all precipitation products (IMD, GPM – IMERG, TRMM, and PERSIANN) during the period of 2000–2018 at basin scale and (b) their Mean Absolute Error (MAE).

document, Figure S2. From the spatial distribution of the CC, it can be observed that PERSIANN-CDR data has lower CC at all the grid points compared to the GPM-IMERGV6 and TRMM-3B42V7. The spatial distribution of the RMSE shows that the percentage of regions with higher MAE is high for PERSIANN-CDR and TRMM-3B42V7 compared to GPM-IMERGV6.

3.3. Evaluation for different seasons

The Indian Meteorological Department classifies four seasons in India, namely spring (March to May), summer (June to September), fall (October to December), and winter (January and February). The SPPs were evaluated separately at each season.

During the spring season, the correlation coefficient for all the products is similar and varies from 0.07 to 0.27, 0.05 to 0.25, and 0.05 to 0.26 for IMERG, TRMM, and PERSIANN, respectively, as can be seen from Figure 10. However, IMERG shows

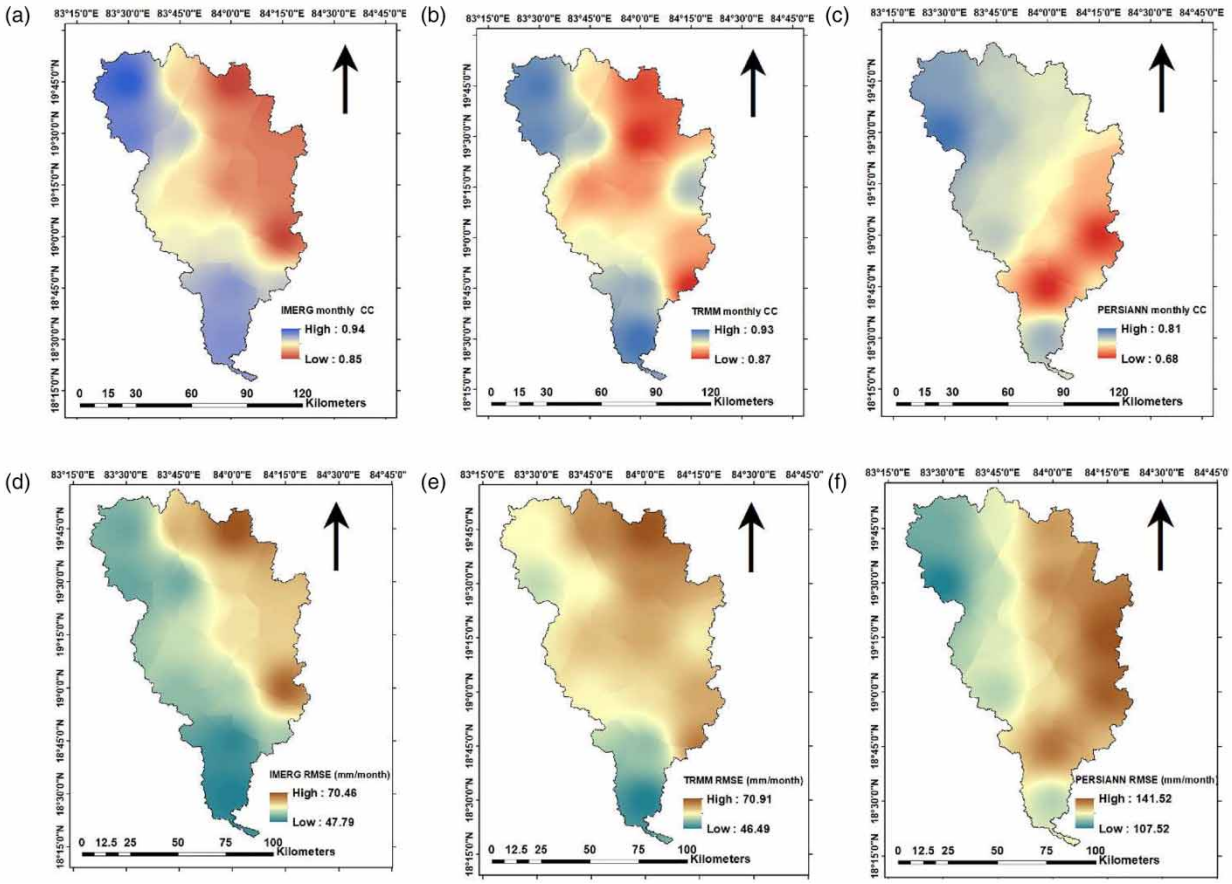

Figure 9 | The spatial distribution of correlation coefficient of (a) IMERG (b) TRMM (c) PERSIANN; root mean square error of (d) IMERG (e) TRMM (f) PERSIANN at monthly scale over the period of 2000–2018. The spatial maps were created from the statistical metrics at 15 grid points using Inverse Distance Weighted interpolation (IDW) in ArcMap.

the lowest RMSE (5.26 to 7.86 mm/day), followed by TRMM (6.43 to 9.66 mm/day). This season, the PERSIANN performed the worst in RMSE (10.38 to 12.45 mm/day). All the products show a similar spatial pattern, with performance decreasing downstream to upstream during the spring season.

Figures 11 and 12 show the spatial variation of CC and RMSE during the monsoon and fall seasons. All the products performed better in the summer and fall seasons. The IMERG (0.21 to 0.4, 0.31 to 0.46) have relatively higher CC than TRMM (0.18 to 0.32, 0.3 to 0.5) and PERSIANN (0.22 to 0.28, 0.28 to 0.43) during the summer and fall seasons.

Contrastingly, during the winter season, the IMERG has the highest RMSE (8.43 to 15.28 mm/day), followed by TRMM (1.91 to 3.92 mm/day) and PERSIANN (1.76 mm/day to 3.31 mm/day). However, IMERG and TRMM have higher CC than PERSIANN during this season, as shown in Figure 13. For a better comparison of the precipitation products with the same color scale, please refer to the supporting document Figures S3, S4, S5, and S6, corresponding to Figures 10–13.

On watershed-scale analysis, it is observed that all the products performed well in the fall and summer seasons, as indicated by higher correlation coefficients. All the products overestimated the mean rainfall during the summer season and underestimated it during the fall and winter. The errors were highest in the PERSIANN product and lowest in IMERG during the spring and summer. The systematic error in IMERG was considerably reduced during the spring season. The TRMM performed relatively better than IMERG during the winter season, as indicated by higher CC and lower percent bias. The detailed results are shown in Table 6.

3.4. Evaluation at the yearly time scale

The annual total precipitation data is obtained from the accumulated total monthly precipitation. The correlation between IMD gridded data and satellite precipitation products was 0.62, 0.62, and 0.23 by TRMM-3B42V7, IMERGV6, and

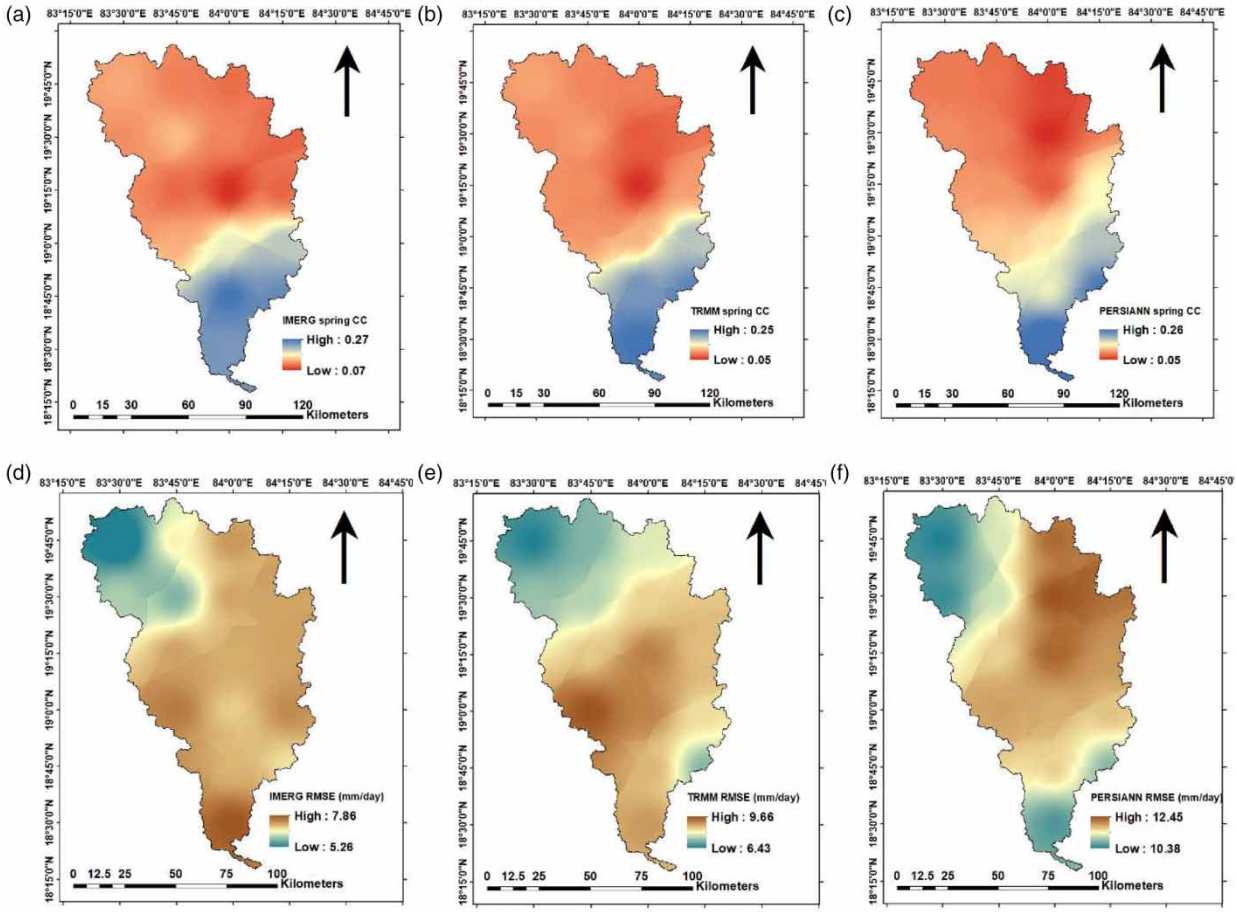

Figure 10 | The spatial distribution of correlation coefficient of (a) IMERG (b) TRMM (c) PERSIANN; root mean square error of (d) IMERG (e) TRMM (f) PERSIANN for spring season over the period of 2000–2018. The spatial maps were created from the statistical metrics at 15 grid points using Inverse Distance Weighted interpolation (IDW) in ArcMap.

PERSIANN-CDR products, respectively, as shown in Table 4. The PERSIANN-CDR data had more significant error values of RMSE, and MAE is 756 mm/yr and 679 mm/yr, respectively, compared to other data sets. GPM-IMERG V6 data product has better error values of 182 mm/yr for RMSE and 160 mm/yr for MAE than the TRMM-3B42V7 product, as shown in Table 4. TRMM-3B42V7 and IMERGV6 data products have slight differences with RMSE and MAE error values, but PERSIANN-CDR data shows the worst performance with the highest error values. The standard deviation for all products is 187, 169, and 304 for TRMM-3B42V7, IMERGV6, and PERSIAN data, respectively. Based on this analysis at the annual time scale, the GPM-IMERGV6 product performs better than the other two products, such as TRMM-3B42V7 and PERSIANN-CDR data products; TRMM-3B42V7 data shows moderate performance.

This study observed the IMD precipitation product; the average annual precipitation is 1,295 mm/y, and minimum and maximum annual precipitation is 917 mm/y (in 2011) and 1,604 mm/y (in 2018), respectively, for 19 years. The average annual precipitations for the TRMM-3B42V7, GPM-IMERGV6 and PERSIANN-CDR satellite products are 1,408 mm/y, 1,345 mm/y, and 1,974 mm/y, respectively. Interestingly, the PERSIANN-CDR has a huge overestimation of 679 mm/year compared to IMD's average annual precipitation (1,295 mm/y).

Based on IMD data, the precipitation increased from south to north, as shown in Figure 14. Earlier studies reported that the rainfall amount decreases with a decrease in vegetation (Hilker *et al.* 2014; Hoscilo *et al.* 2015; Nega *et al.* 2019). A large amount of precipitation in the upper portion of the river basin may be attributed to dense forests. The southern part of the basin falls on the leeward side of hills in the river basin. This resulted in lower rainfall in this region. A similar pattern was observed by all satellite precipitation products except for the PERSIANN-CDR data product; it captured the lower precipitation pattern in the upper and lower portion of the river basin and captured the higher precipitation pattern in the east

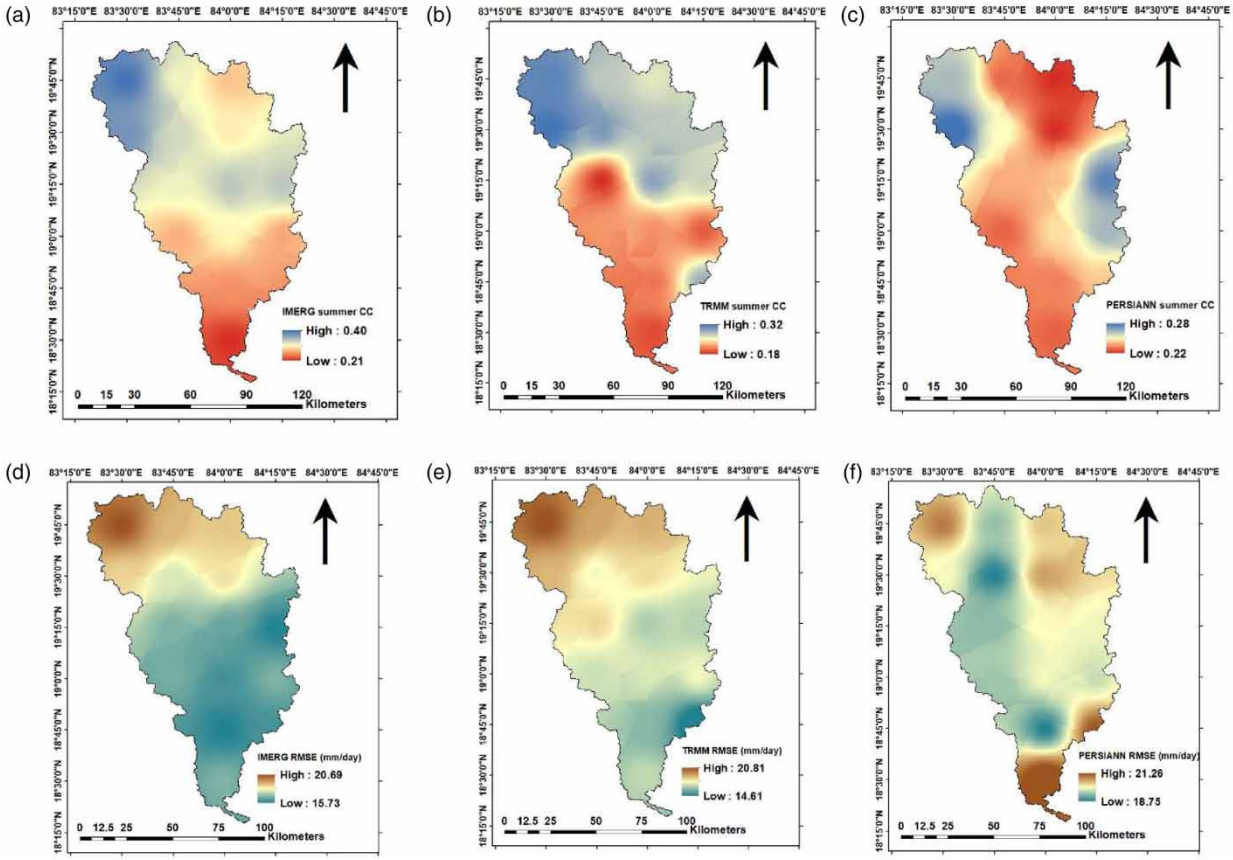

Figure 11 | The spatial distribution of correlation coefficient of (a) IMERG (b) TRMM (c) PERSIANN; root mean square error of (d) IMERG (e) TRMM (f) PERSIANN for the summer season over the period of 2000–2018. The spatial maps were created from the statistical metrics at 15 grid points using Inverse Distance Weighted interpolation (IDW) in ArcMap.

portion of the river basin. On the quantitative aspects, all satellite data products overestimated the average annual precipitation concerning the IMD dataset from 2000 to 2018 at all 15 grid points except the IMERG V6 product, wherein there is some evidence of underestimation at a few points.

Figure 15 shows that the correlation is well captured at the yearly time scale at north and south compared to the middle part of the study area by GPM-IMERGV6 and TRMM-3B42V7 products. PERSIANN-CDR data has a negative correlation value at four grid locations, showing a low correlation against the IMD gridded data at this scale. For a direct comparison of the precipitation products with the same scale, please refer to the supporting document Figure S7. Comparing all products, GPM-IMERGV6 has the highest correlation value (0.54), which is very close to the TRMM-3B42V7 correlation value (0.52). The MAE values were comparatively high for the PERSIANN-CDR dataset for the entire basin, whereas the GPM-IMERGV6 product showed fewer MAE error values for most of the study area. The GPM-IMERGV6 product has low RMSE and low deviation values compared to other products, as shown in Table 4.

Overall, the GPM-IMERGV6 product performs better than the other products based on the statistical metrics at all times.

3.5. Hydrological model evaluation

3.5.1. Scenario A

Before calibrating the model, the sensitivity analysis was performed to identify the sensitive parameters with a global sensitivity analysis method using the SUFI-2 algorithm (part of the SWAT-CUP tool). Out of several parameters, 18 were selected (shown in Table 7) for streamflow simulation based on other literature for the study region (Setti *et al.* 2020a, 2020b). The model was calibrated at daily and monthly time scales; at each scale, 18 parameters were used for model calibration.

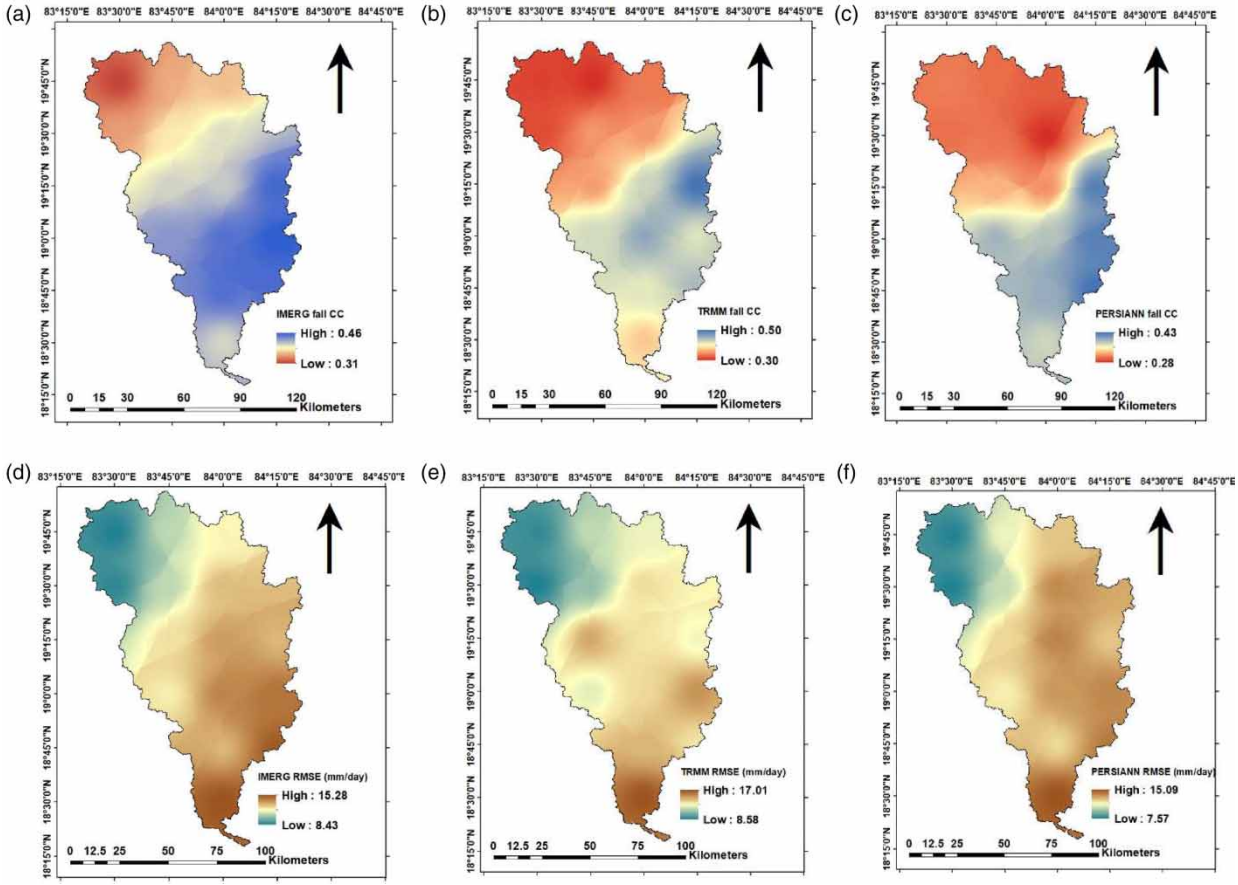

Figure 12 | The spatial distribution of correlation coefficient of (a) IMERG (b) TRMM (c) PERSIANN; root mean square error of (d) IMERG (e) TRMM (f) PERSIANN for the fall season over the period of 2000–2018. The spatial maps were created from the statistical metrics at 15 grid points using Inverse Distance Weighted interpolation (IDW) in ArcMap.

Both at daily and monthly scales, model calibration and validation results were satisfactory according to the values provided (Moriasi *et al.* 2007; Tuo *et al.* 2016). The values of NSE for calibration (validation) at monthly and daily scales were found to be equal to 0.86(0.84) and 0.69(0.68), respectively, showing that the model can capture the streamflow pattern and values. The correlation coefficient values were 0.78–0.82 and 0.91–0.92 on daily and monthly scales, respectively. The PBIAS values show an overestimation in the model simulation at both time scales; however, the values are within the limits prescribed by Moriasi *et al.* (2007). The scatter plot of the model calibrated using IMD during the validation period at daily and monthly scales is shown in Figure 16. Results showed that the model had been calibrated satisfactorily.

When the calibrated model was re-run with SPPs as inputs at the daily scale, the model's performance did not show encouraging results. The NSE ranges from 0.34 (PERSIANN CDR) to 0.58 (GPM) when these SPPs are used to drive the model. At the monthly scale, the results from the model with TRMM-3B42V7 and GPM-IMERG V6 as inputs show that the model performance is satisfactory in terms of NSE and PBIAS and good in terms of CC (see Figure 17 and Table 8). These results show that the model can capture the overall streamflow pattern to an acceptable level. However, when PERSIANN-CDR was used as the input precipitation dataset, the model performance in NSE and PBIAS was unsatisfactory. The scatter plots (see Figure 17) show a considerable overestimation of the streamflow stemming from the rainfall estimates by the SPPs. Among the satellite precipitation products compared in this study, GPM-IMERGV6 shows better performance than the TRMM-3B42V7 and PERSIANN-CDR data sets.

4. DISCUSSION

This paper comprehensively analyses the reliability and applicability of the latest satellite precipitation datasets (PERSIANN-CDR, TRMM-3B42V7–3B42, GPM-IMERGV6) against the gauge based gridded datasets reported for a cyclone-prone coastal

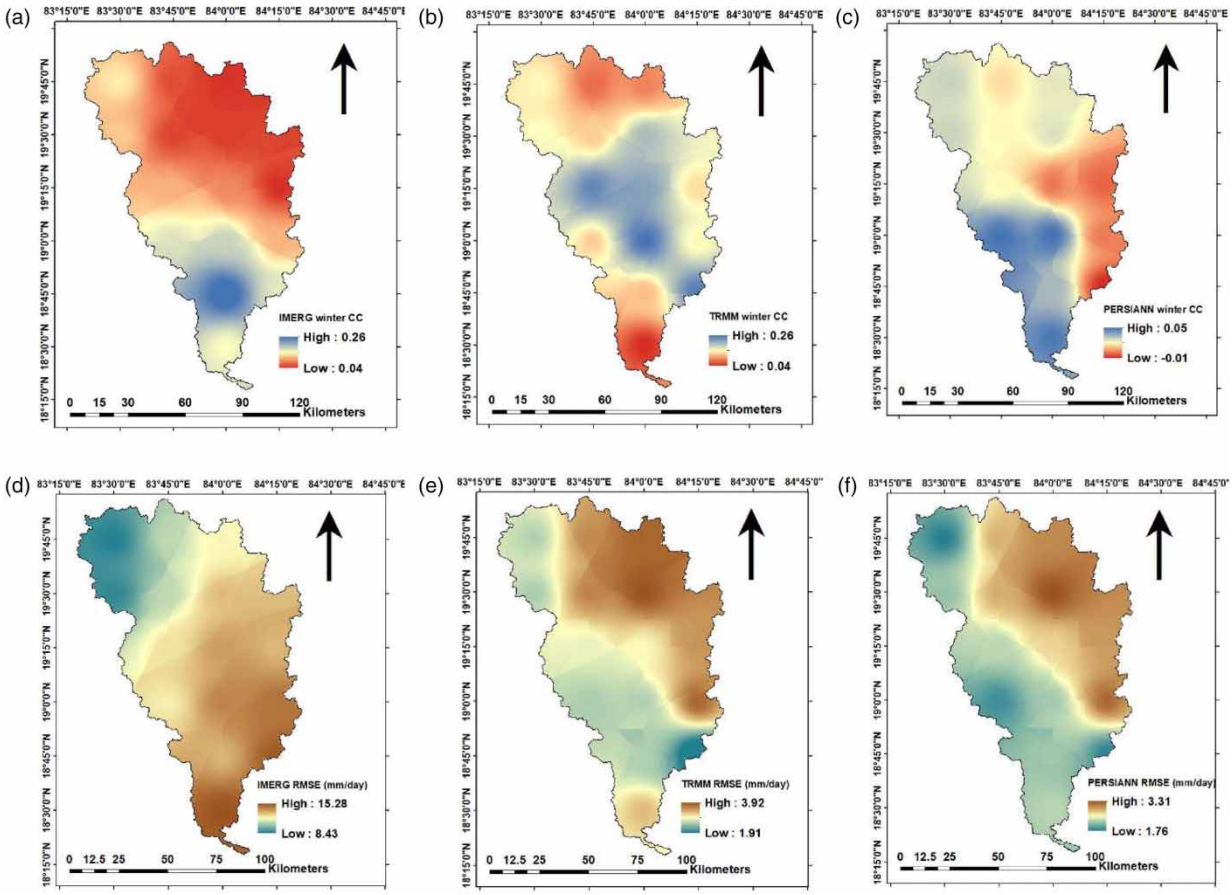

Figure 13 | The spatial distribution of correlation coefficient of (a) IMERG (b) TRMM (c) PERSIANN; root mean square error of (d) IMERG (e) TRMM (f) PERSIANN for the winter season over the period of 2000–2018. The spatial maps were created from the statistical metrics at 15 grid points using Inverse Distance Weighted interpolation (IDW) in ArcMap.

river basin of peninsular India. For this purpose, the evaluation and comparison of the precipitation estimates were performed at different temporal scales. Following this, the spatial comparison was studied along with the suitability of each product to drive a hydrologic model with the SWAT model at daily and monthly time steps

At the daily scale, the performance of the SPPs varied for different rainfall intensity ranges, even though the PERSIANN-CDR is closer to gauge precipitation data when the precipitation range is very light rainfall, for moderate and heavy rainfall events, 3B43V7 and GPM-IMERG V6 were closer to the gauge estimates than PERSIANN-CDR. All the SPPs investigated in this study showed an overestimation of rainfall and further comparison among the precipitation data sets. The PERSIANN-CDR data tend to have higher FAR values for all rainfall thresholds, indicating a high tendency for false alarms. Similarly, in CSI values, the PERSIANN-CDR data shows a low success rate compared to the TRMM-3B42V7 and GPM-IMERGV6 for different intensity ranges. It was observed that the POD for all SPPs varies with the space and intensity of the rainfall. The POD is high in the northwestern part of the catchment and low in the southern part of the catchment. It was also observed that all the SPPs have lower POD in the eastern part of the catchment, which is prone to frequent cyclones (Setti *et al.* 2020a, 2020b; Yeditha *et al.* 2020), particularly for heavy rainfall (>50 mm/day). The FAR analysis revealed that all the SPPs have a significant level of false detection. It would be interesting to explore a detailed evaluation of these products focusing on extreme events associated with a cyclone event at the basin.

Comparing the SPPs at the monthly scale, the correlation between reference data and TRMM-3B42V7, GPM-IMERGV6, and PERSIANN-CDR products was found to be 0.94, 0.93, and 0.78, respectively, indicating the TRMM-3B42V7 and GPM-IMERG V6 data products were better correlated with IMD gridded data compared to the PERSIANN-CDR data product. This shows that the TRMM-3B42V7 and GPM-IMERGV6-based products can capture the overall seasonal pattern in the

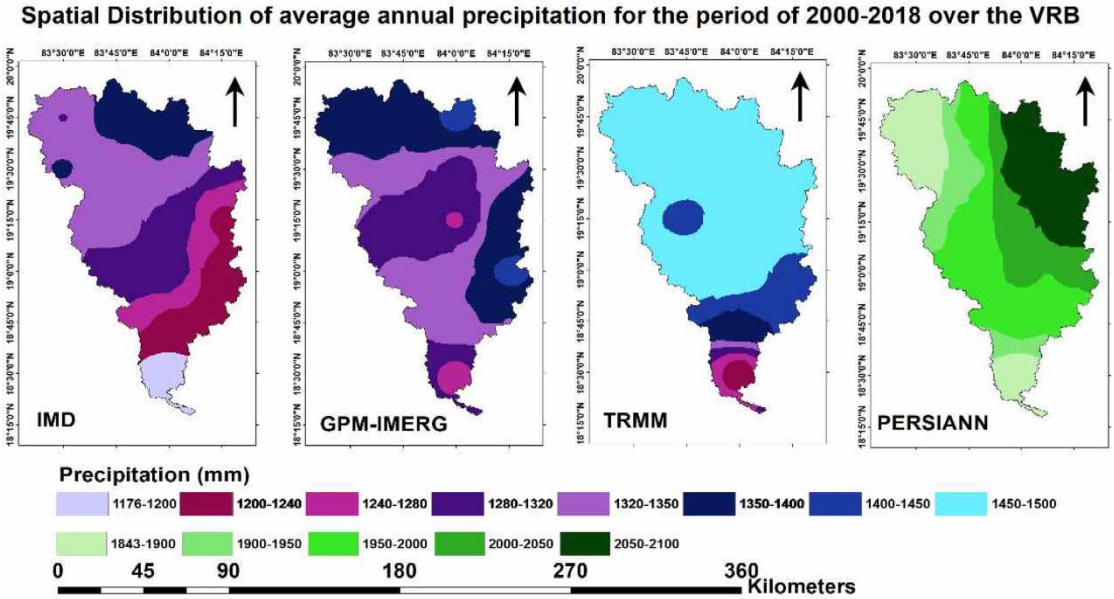

Figure 14 | Comparison of Spatial Distribution of average annual precipitation of TRMM, GPM-IMERG, and PERSIANN satellite precipitation products with IMD gridded precipitation in the Vamsadhara River Basin from 2000 to 2018 at grid scale.

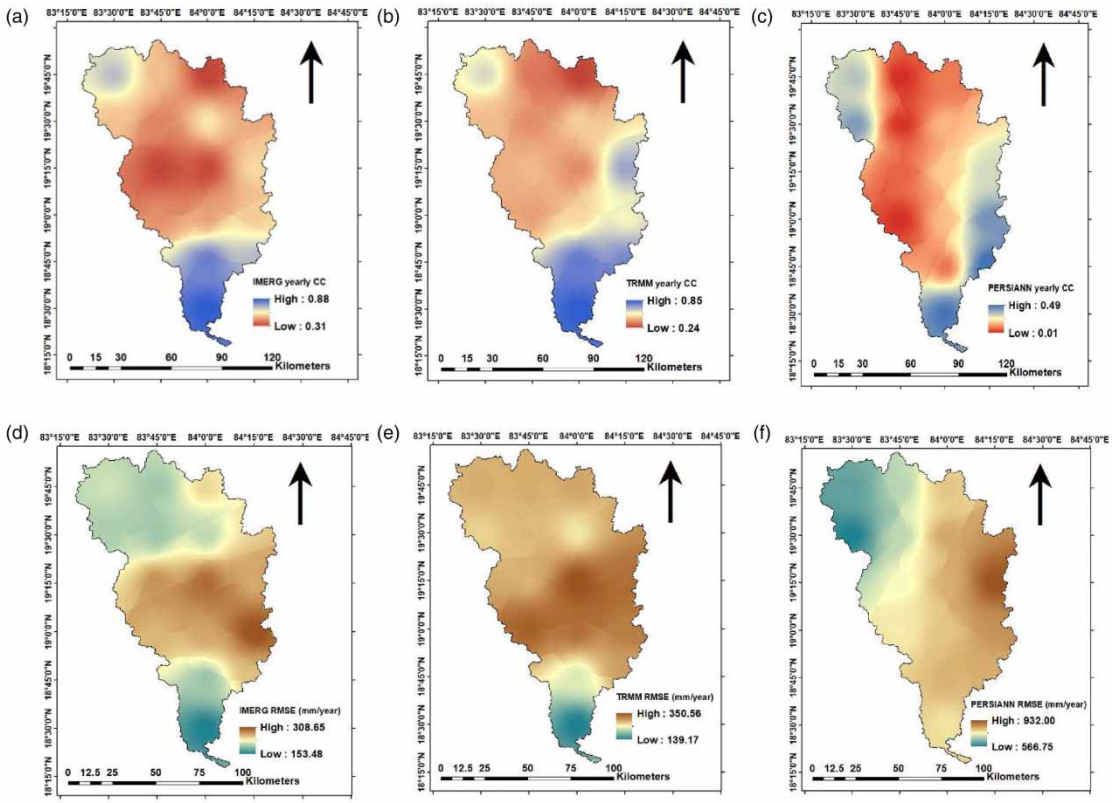

Figure 15 | The spatial distribution of correlation coefficient of (a) IMERG (b) TRMM (c) PERSIANN; root mean square error of (d) IMERG (e) TRMM (f) PERSIANN at yearly scale over the period of 2000–2018. The spatial maps were created from the statistical metrics at 15 grid points using Inverse Distance Weighted interpolation (IDW) in ArcMap.

Table 7 | Hydrological parameters used during sensitive analysis and their description

Sl.No	Parameters	Description
1	RCHRG_DP	Deep aquifer percolation fraction
2	ESCO	Soil evaporation compensation factor
3	SOL_K	Soil hydraulic conductivity (mm/hr)
4	SOL_AWC	Available water capacity of the soil layer (mm)
5	CN2	Curve number
6	LAT_TTIME	Lateral flow travel time (days)
7	GW_DELAY	Groundwater delay (days)
8	CH_N2	Manning's 'n' value for the main channel
9	SLSUBBSN	Average slope length (m)
10	HRU_SLP	Average slope steepness (m/m)
11	EPCO	Plant evaporation compensation factor
12	CH_K2	Hydraulic conductivity of main channel (mm/hr)
13	GW_REVAP	Groundwater recap coefficient
14	GWQMN	Threshold depth of water in the shallow aquifer (mm)
15	ALPHA_BF	Baseflow alpha factor (days)
16	REVAPMN	Threshold depth of water in the shallow aquifer for recap to occur (mm)
17	OV_N	Manning's 'n' value for overland flow
18	SURLAG	Surface runoff lag time

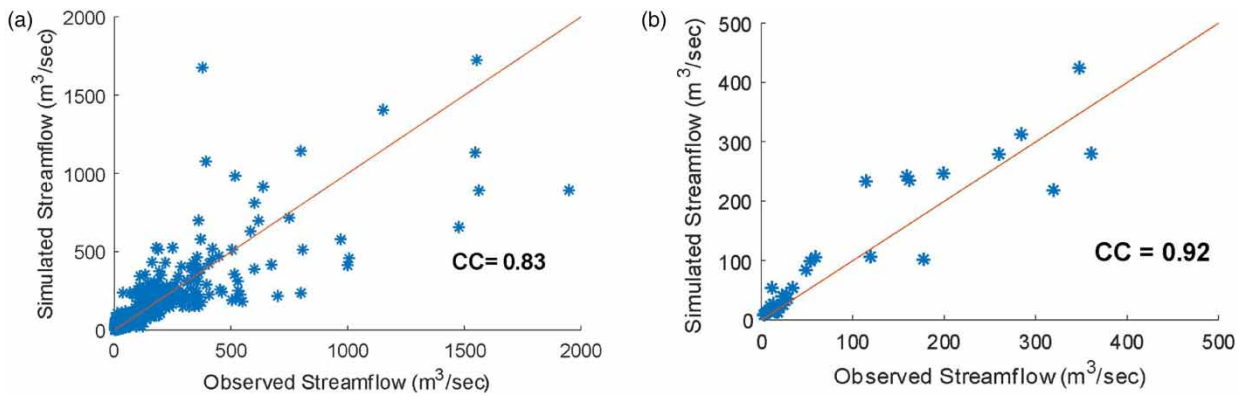

Figure 16 | Model validation results from the SWAT model run with the IMD precipitation data set at (a) daily scale and (b) monthly scale. The red line shows the X = Y line.

study region and, therefore, can be used for modeling studies. Comparing satellite and gauged-based precipitation datasets at an annual scale, both TRMM-3B42V7 and GPM-IMERGV6 demonstrate better performance than PERSIANN-CDR in terms of all criteria over the study region. In addition, TRMM-3B42V7 and GPM-IMERGV6 slightly overestimate precipitation, while PERSIANN-CDR shows a substantial overestimation. An interesting finding from this analysis was that the SPP's performance (in terms of statistical analysis and hydrologic model results) was better at a monthly scale than the daily and yearly scales. This could be because the seasonal mean cycle highly dominates the overall variance, thereby giving better results at a monthly scale. An interesting exercise would be to evaluate the performance of these SPPs after removing the seasonal means. Further, Hosseini-Moghari & Tang (2020) suggest that these SPPs are generally adjusted at a monthly scale, showing better results on a monthly scale.

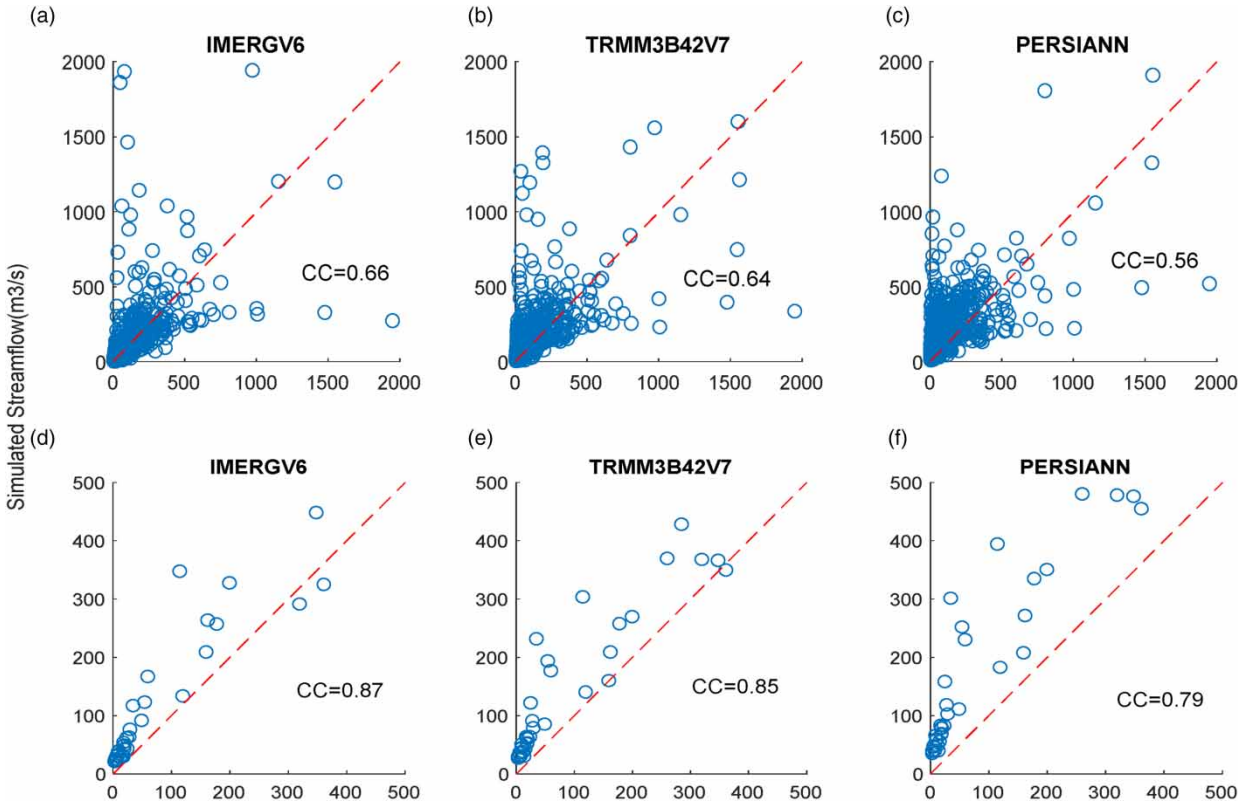

Figure 17 | Scatter plot between observed and model simulated streamflow for Scenario A during the validation period using different SPPs (a–c) daily scale (d–f) monthly scale. The red line shows the X = Y line.

Table 8 | SWAT model performance in simulating stream flow under Scenario A (IMD precipitation based SWAT model is calibrated and validated and the same is re-run with other precipitation products)

			Scenario A		
	IMD Results		Calibrated model re-run by other precipitation products (Validation Period)		
Statistical Measures	Calibration Period	Validation Period	TRMM	GPM-IMERG	PERSIANN
Daily Scale					
NSE	0.69	0.68	0.32	0.38	0.28
CC	0.82	0.78	0.64	0.66	0.56
Pbias	−1.7	−8.4	−23.4	−25	−39.2
Monthly Scale					
NSE	0.86	0.84	0.53	0.66	0.31
CC	0.92	0.91	0.85	0.87	0.79
Pbias	−3.6	−16.8	−67.2	−63.5	−88.1

All the products performed relatively better on a seasonal scale during the wet season (summer and fall) than the dry seasons at pixel and basin scales. Similar results were also reported at the Tibetan Plateau (Alazzy *et al.* 2017). However, all the SPPs overestimated the amount of rainfall during the summer season. This is probably because raindrops evaporate in the semi-arid climate before reaching the surface (Tesfagiorgis *et al.* 2011). During the winter season, TRMM is found to be relatively better than the other products. The PERSIANN-CDR performed consistently worse in all the seasons. Our results were

consistent with the previous study (Moazami *et al.* 2016; Chen *et al.* 2020a; Gadouali & Messouli 2020). Chen *et al.* (2020a) also reported that the PERSIANN-CDR failed to capture seasonal precipitation trends and performed worse among the other products (CHIRPS and TRMM) over an arid mountainous area in China.

Comparing the performance of the TRMM and GPM products, it was observed that the latter showed a better ability to capture different rainfall intensities more accurately than the former. Further, the error statistics were comparatively lower for GPM than the TRMM- 3B42V7. The improved performance of the IMERG V6 product compared to its predecessor TRMM-3B42V7 can be attributed to the changes, such as in the retrieval algorithm used in Version 6. Huffman *et al.* (2015) report that the retrieval algorithm of IMERG V06 uses a new morphing approach and involves some refinements in the CMORPH-Kalman Filter. Further, Anjum *et al.* 2019; Hosseini-Moghari & Tang, (2020) also showed that GPM-IMERG V6 performs better than its predecessor in the Iran region.

The results of streamflow simulation using SWAT under the two scenarios in this study suggest that: In scenario A, TRMM-3B43V7 and GPM-IMERG V6-derived simulations with IMD benchmarked model parameter values yield comparable performance to benchmark model in the calibration and validation period. By contrast, the PERSIANN-CDR product yields the worst model performance and has little potential for use in hydrological simulation over the study region.

In Scenario B, all SPP-based model simulations show significantly improved performance after recalibration both in the calibration and validation period; however, PERSIANN-CDR still performed worse than the other two products (refer to Table S1 and Figure S1).

On comparing both scenarios, we observed that the model performance improved in Scenario B compared to Scenario A at a daily scale, implying that individual model calibration improved the streamflow simulation. However, stream flow simulations have no significant improvement at the monthly time scale. This could be attributed to the fact that there is good agreement between IMD precipitation data and TRMM and GPM data sets monthly than at the daily scale. These results imply that the application of SPPs for hydrological models needs daily calibration with individual precipitation datasets. In contrast, at the monthly time scale, the IMD driven model is sufficient for streamflow simulation using SPPs.

In this study, the IMD gridded dataset is the ground truth data. Since the IMD dataset is interpolated data sampled at 0.25°, this would undoubtedly add uncertainty to the error estimates obtained from the study and, thereby, the quality of the satellite data products.

5. CONCLUSION

Satellite precipitation products (SPPs) are an effective alternative for rainfall data and streamflow simulations at global and regional scales, thereby helping water management practices and decisions. Despite the superiority of the SPPs over the gauge data (in terms of temporal resolution, spatial coverage, and availability of data), their accuracy has to be evaluated at regional scales. This study evaluated three recent precipitation products (IMERGV6, TRMM-3B42V7, PERSIANN-CDR) using a gauge-based precipitation product for 2000–2018 using statistical metrics and a hydrological model over a cyclone-prone basin in southeast India. The salient findings from the study can be summarized as follows.

1. Of the different precipitation products in the present study, IMERGV6 shows reliability compared to the other products in capturing extreme events and is found to be suitable for driving hydrological models. Further, the accuracy of the SPPs is moderate at daily time scales and good at monthly time scales, indicating that these products can be used reliably for water balance studies at coarser time scales; however, it needs appropriate correction before being applied for short-term flood modeling.
2. The grid level evaluation of the SPPs showed that the IMERGV6 precipitation product has higher CC, lower RMSE, and higher POD and CSI than TRMM-3B42V7 and PERSIANN-CDR.
3. The SWAT model calibration and validation using individual precipitation products showed that the satellite data IMERGV6 and TRMM-3B42V7 could drive the hydrological model. The results were comparable to those of the ground-based model. However, the results using the PERSIANN-CDR were not convincing as the satellite data tend to overestimate precipitation in the study region.

Overall, among the three SPPs, GPM-IMERGV6 shows comparatively better performance than the other products. Hence, it could potential alternative for a data-scarce cyclone-dominated river basin in southeast India. Future studies could investigate the spatio-temporal characteristics of specific cyclones over this region and the ability of the SPPs to capture the same.

ACKNOWLEDGEMENTS

The Early Career Research Award has supported this research under SERB, India, under grant No. ECRA/2016/01721. The authors are also grateful for the partial support from the Inspire Faculty grant held by Dr Maheswaran from DST. The authors would like to thank the anonymous reviewers.

DATA AVAILABILITY STATEMENT

All relevant data are included in the paper or its Supplementary Information.

CONFLICT OF INTEREST

The authors declare there is no conflict.

REFERENCES

Abbaspour, K. C., Yang, J., Maximov, I., Siber, R., Bogner, K., Mieleitner, J., Zobrist, J. & Srinivasan, R. 2007 Modelling hydrology and water quality in the pre-alpine/alpine Thur watershed using SWAT. *Journal of Hydrology* **333**, 413–430. https://doi.org/10.1016/j.jhydrol.2006.09.014.

Abbaspour, K. C., Rouholahnejad, E., Vaghefi, S., Srinivasan, R., Yang, H. & Kløve, B. 2015 A continental-scale hydrology and water quality model for Europe: calibration and uncertainty of a high-resolution large-scale SWAT model. *Journal of Hydrology* **524**, 733–752. https://doi.org/10.1016/j.jhydrol.2015.03.027.

Agarwal, A., Marwan, N., Maheswaran, R., Merz, B. & Kurths, J. 2018 Quantifying the roles of single stations within homogeneous regions using complex network analysis. *Journal of Hydrology* **563**, 802–810. https://doi.org/10.1016/j.jhydrol.2018.06.050.

Alazzy, A. A., Lü, H., Chen, R., Ali, A. B., Zhu, Y. & Su, J. 2017 Evaluation of satellite precipitation products and their potential influence on hydrological modeling over the ganzi river basin of the Tibetan plateau [WWW document]. *Advances in Meteorology*. https://doi.org/10.1155/2017/3695285

Anjum, M. N., Ahmad, I., Ding, Y., Shangguan, D., Zaman, M., Ijaz, M. W., Sarwar, K., Han, H. & Yang, M. 2019 Assessment of IMERG-V06 precipitation product over different hydro-climatic regimes in the Tianshan Mountains, North-Western China. *Remote Sensing* **11** (19), 2314. https://doi.org/10.3390/rs11192314

Ashouri, H., Hsu, K.-L., Sorooshian, S., Braithwaite, D. K., Knapp, K. R., Cecil, L. D., Nelson, B. R. & Prat, O. P. 2015 PERSIANN-CDR: Daily precipitation climate data record from multisatellite observations for hydrological and climate studies. *Bulletin of the American Meteorological Society* **96**, 69–83. https://doi.org/10.1175/BAMS-D-13-00068.1.

Beck, H. E., Vergopolan, N., Pan, M., Levizzani, V., van Dijk, A. I. J. M., Weedon, G. P., Brocca, L., Pappenberger, F., Huffman, G. J. & Wood, E. F. 2017 Global-scale evaluation of 22 precipitation datasets using gauge observations and hydrological modeling. *Hydrology and Earth System Sciences* **21**, 6201–6217. https://doi.org/10.5194/hess-21-6201-2017.

Belabid, N., Zhao, F., Brocca, L., Huang, Y. & Tan, Y. 2019 Near-real-time flood forecasting based on satellite precipitation products. *Remote Sensing* **11**, 252. https://doi.org/10.3390/rs11030252.

Beria, H., Nanda, T., Singh Bisht, D. & Chatterjee, C. 2017 Does the GPM mission improve the systematic error component in satellite rainfall estimates over TRMM? an evaluation at a pan-India scale. *Hydrology and Earth System Sciences* **21**, 6117–6134. https://doi.org/10.5194/hess-21-6117-2017.

Bharti, V. & Singh, C. 2015 Evaluation of error in TRMM 3b42v7 precipitation estimates over the himalayan region: EVALUATION OF ERROR IN TRMM 3b42v7. *Journal of Geophysical Research: Atmospheres* **120**, 12458–12473. https://doi.org/10.1002/2015JD023779.

Bitew, M. M. & Gebremichael, M. 2011 Evaluation of satellite rainfall products through hydrologic simulation in a fully distributed hydrologic model: SATELLITE RAINFALL HYDROLOGIC SIMULATION. *Water Resources Research* **47**. https://doi.org/10.1029/2010WR009917.

Chen, C., Li, Z., Song, Y., Duan, Z., Mo, K., Wang, Z. & Chen, Q. 2020a Performance of multiple satellite precipitation estimates over a typical arid mountainous area of China: spatiotemporal patterns and extremes. *Journal of Hydrometeorology* **21**, 533–550. https://doi.org/10.1175/JHM-D-19-0167.1.

Chen, S., Zhang, L., Zhang, Y., Guo, M. & Liu, X. 2020b Evaluation of tropical rainfall measuring mission (TRMM) satellite precipitation products for drought monitoring over the middle and lower reaches of the Yangtze River Basin, China. *Journal of Geographical Sciences* **30**, 53–67. https://doi.org/10.1007/s11442-020-1714-y.

Dandridge, C., Lakshmi, V., Bolten, J. & Srinivasan, R. 2019 Evaluation of satellite-based rainfall estimates in the Lower Mekong River Basin (Southeast Asia). *Remote Sensing* **11**, 2709. https://doi.org/10.3390/rs11222709.

Dars, G. H., Strong, C., Kochanski, A. K., Ansari, K. & Ali, S. H. 2020 The spatiotemporal variability of temperature and precipitation over the upper Indus basin: an evaluation of 15 year WRF simulations. *Applied Sciences* **10**, 1765. https://doi.org/10.3390/app10051765.

Dhanesh, Y., Bindhu, V. M., Senent-Aparicio, J., Brighenti, T. M., Ayana, E., Smitha, P. S., Fei, C. & Srinivasan, R. 2020 A comparative evaluation of the performance of CHIRPS and CFSR data for different climate zones using the SWAT model. *Remote Sensing* **12**, 3088. https://doi.org/10.3390/rs12183088.

Dinku, T., 2020 The Value of Satellite Rainfall Estimates in Agriculture and Food Security. In: *Satellite Precipitation Measurement: Volume 2, Advances in Global Change Research* (Levizzani, V., Kidd, C., Kirschbaum, D. B., Kummerow, C. D., Nakamura, K. & Turk, F. J., eds.). Springer International Publishing, Cham, pp. 1113–1129. https://doi.org/10.1007/978-3-030-35798-6_32.

Fuka, D. R., Walter, M. T., MacAlister, C., Degaetano, A. T., Steenhuis, T. S. & Easton, Z. M. 2014 Using the climate forecast system reanalysis as weather input data for watershed models: USING CFSR AS WEATHER INPUT DATA FOR WATERSHED MODELS. *Hydrological Processes* **28**, 5613–5623. https://doi.org/10.1002/hyp.10073.

Gadouali, F. & Messouli, M. 2020 Evaluation of multiple satellite-derived rainfall products over Morocco. *International Journal of Hydrology Science and Technology* **10**, 72–89. https://doi.org/10.1504/IJHST.2020.104988.

Guntu, R. K., Rathinasamy, M., Agarwal, A. & Sivakumar, B. 2020 Spatiotemporal variability of Indian rainfall using multiscale entropy. *Journal of Hydrology* **587**, 124916. https://doi.org/10.1016/j.jhydrol.2020.124916

Guo, J. & Su, X. 2019 Parameter sensitivity analysis of SWAT model for streamflow simulation with multisource precipitation datasets. *Hydrology Research* **50**, 861–877. https://doi.org/10.2166/nh.2019.083.

Hargreaves, G. H. & Samani, Z. A. 1985 Reference crop evapotranspiration from temperature. *Applied engineering in agriculture* **1** (2), 96–99. doi: 10.13031/2013.26773.

Hilker, T., Lyapustin, A. I., Tucker, C. J., Hall, F. G., Myneni, R. B., Wang, Y., Bi, J., Mendes de Moura, Y. & Sellers, P. J. 2014 Vegetation dynamics and rainfall sensitivity of the Amazon. *PNAS* **111**, 16041–16046.

Himanshu, S. K., Pandey, A. & Patil, A. 2018 Hydrologic evaluation of the TMPA-3b42v7 precipitation data Set over an agricultural watershed using the SWAT model. *Journal of Hydrologic Engineering* **23**, 05018003. https://doi.org/10.1061/(ASCE)HE.1943-5584.0001629.

Hoscilo, A., Balzter, H., Bartholomé, E., Boschetti, M., Brivio, P. A., Brink, A., Clerici, M. & Pekel, J. F. 2015 A conceptual model for assessing rainfall and vegetation trends in sub-Saharan Africa from satellite data. *International Journal of Climatology* **35**, 3582–3592. https://doi.org/10.1002/joc.4231.

Hosseini-Moghari, S. M. & Tang, Q. 2020 Validation of GPM IMERG V05 and V06 precipitation products over Iran. *Journal of Hydrometeorology* **21** (5), 1011–1037. https://doi.org/10.1175/JHM-D-19-0269.1

Hou, A. Y., Kakar, R. K., Neeck, S., Azarbarzin, A. A., Kummerow, C. D., Kojima, M., Oki, R., Nakamura, K. & Iguchi, T. 2014 The global precipitation measurement mission. *Bulletin of the American Meteorological Society* **95**, 701–722. https://doi.org/10.1175/BAMS-D-13-00164.1.

Huffman, G. J., Bolvin, D. T., Nelkin, E. J., Wolff, D. B., Adler, R. F., Gu, G., Hong, Y., Bowman, K. P. & Stocker, E. F. 2007 The TRMM multisatellite precipitation analysis (TMPA): quasi-Global, multiyear, combined-Sensor precipitation estimates at fine scales. *Journal of Hydrometeorology* **8**, 38–55. https://doi.org/10.1175/JHM560.1.

Huffman, G. J., Bolvin, D. T., Nelkin, E. J. & Tan, J. 2015 Integrated Multi-satellitE Retrievals for GPM (IMERG) technical documentation. Nasa/Gsfc Code, 612 (47), p.2019. https://gpm.nasa.gov/sites/default/files/document_files/IMERG_doc_190909.pdf

Jamro, S., Dars, G. H., Ansari, K. & Krakauer, N. Y. 2019 Spatio-Temporal variability of drought in Pakistan using standardized precipitation evapotranspiration index. *Applied Sciences* **9**, 4588. https://doi.org/10.3390/app9214588.

Krisnayanti, D. S., Bunganaen, W., Frans, J. H., Seran, Y. A. & Legono, D. 2021 Curve number estimation for ungauged watershed in semi-arid region. *Civil Engineering Journal* **7** (6), 1070–1083. Doi: 10.28991/cej-2021-03091711.

Kumar, P. & Singh, A. K. 2022 A comparison between MLR, MARS, SVR and RF techniques: hydrological time-series modeling. *Journal of Human, Earth, and Future* **3** (1), 90–98. https://www.hefjournal.org/index.php/HEF/article/view/137

Le, M.-H., Lakshmi, V., Bolten, J. & Bui, D. D. 2020 Adequacy of satellite-derived precipitation estimate for hydrological modeling in Vietnam basins. *Journal of Hydrology* **586**, 124820. https://doi.org/10.1016/j.jhydrol.2020.124820.

Maggioni, V., Meyers, P. C. & Robinson, M. D. 2016 A review of merged high-Resolution satellite precipitation product accuracy during the tropical rainfall measuring mission (TRMM) Era. *Journal of Hydrometeorology* **17**, 1101–1117. https://doi.org/10.1175/JHM-D-15-0190.1.

Mishra, A. K. 2019 On remote sensing of convective clouds over Indian continent and quantification of their variability in a warming environment. *International Journal of Remote Sensing* **40**, 2830–2840. https://doi.org/10.1080/01431161.2018.1533658.

Moazami, S., Golian, S., Hong, Y., Sheng, C. & Kavianpour, M. R. 2016 Comprehensive evaluation of four high-resolution satellite precipitation products under diverse climate conditions in Iran. *Hydrological Sciences Journal* **61**, 420–440. https://doi.org/10.1080/02626667.2014.987675.

Monteith, J. L. 1965 *Evaporation and environment*. In Symposia of the society for experimental biology, Vol. 19. Cambridge University Press, Cambridge, UK, pp. 205–234.

Moriasi, D., Arnold, J., Van Liew, M., Bingner, R., Harmel, R. D. & Veith, T. 2007 Model evaluation guidelines for systematic quantification of accuracy in watershed simulations. *Transactions of the ASABE* **50**. https://doi.org/10.13031/2013.23153.

Nash, J. E. & Sutcliffe, J. V. 1970 River flow forecasting through conceptual models part I- A discussion of principles. *Journal of Hydrology* **10**, 282–290. https://doi.org/10.1016/0022-1694(70)90255-6

Nega, W., Hailu, B. T. & Fetene, A. 2019 An assessment of the vegetation cover change impact on rainfall and land surface temperature using remote sensing in a subtropical climate, Ethiopia. *Remote Sensing Applications: Society and Environment* **16**, 100266. https://doi.org/10.1016/j.rsase.2019.100266.

Nguyen, P., Ombadi, M., Sorooshian, S., Hsu, K., AghaKouchak, A., Braithwaite, D., Ashouri, H. & Thorstensen, A. R. 2018 The PERSIANN family of global satellite precipitation data: a review and evaluation of products. *Hydrology and Earth System Sciences* **22**, 5801–5816. https://doi.org/10.5194/hess-22-5801-2018.

Niyogi, D., Osuri, K. K., Busireddy, N. K. R. & Nadimpalli, R. 2020 Timing of rainfall occurrence altered by urban sprawl. *Urban Climate* **33**, 100643. https://doi.org/10.1016/j.uclim.2020.100643.

Ojha, S. S., Singh, V. & Roshni, T. 2021 Comparison of meteorological drought using SPI and SPEI. *Civil Engineering Journal* **7** (12), 2130–2149. Doi: 10.28991/cej-2021-03091783.

Pai, D. S., Sridhar, L., Rajeevan, M., Sreejith, O. P., Satbhai, N. S. & Mukhopadyay, B. 2014 Development of a new high spatial resolution (0.25° × 0.25°) Long Period (1901-2010) daily gridded rainfall data set over India and its comparison with existing data sets over the region, 18.

Prakash, S., Mitra, A. K., AghaKouchak, A., Liu, Z., Norouzi, H. & Pai, D. S. 2018 A preliminary assessment of GPM-based multi-satellite precipitation estimates over a monsoon dominated region. *Journal of Hydrology* **556**, 865–876. https://doi.org/10.1016/j.jhydrol.2016.01.029.

Priestley, C. H. B. & Taylor, R. J. 1972 On the assessment of surface heat flux and evaporation using large-scale parameters. *Monthly weather review* **100** (2), 81–92.

Rathinasamy, M., Khosa, R., Adamowski, J., Ch, S., Partheepan, G., Anand, J & Narsimlu, B. 2014 Wavelet-based multiscale performance analysis: An approach to assess and improve hydrological models. *Water Resources Research* **50** (12), 9721–9737. https://doi.org/10.1002/2013WR014650

Ren, P., Li, J., Feng, P., Guo, Y. & Ma, Q. 2018 Evaluation of multiple satellite precipitation products and their Use in hydrological modelling over the Luanhe River Basin, China. *Water* **10**, 677. https://doi.org/10.3390/w10060677.

Saha, S., Moorthi, S., Pan, H.-L., Wu, X., Wang, J., Nadiga, S., Tripp, P., Kistler, R., Woollen, J., Behringer, D., Liu, H., Stokes, D., Grumbine, R., Gayno, G., Wang, J., Hou, Y.-T., Chuang, H., Juang, H.-M. H., Sela, J., Iredell, M., Treadon, R., Kleist, D., Van Delst, P., Keyser, D., Derber, J., Ek, M., Meng, J., Wei, H., Yang, R., Lord, S., van den Dool, H., Kumar, A., Wang, W., Long, C., Chelliah, M., Xue, Y., Huang, B., Schemm, J.-K., Ebisuzaki, W., Lin, R., Xie, P., Chen, M., Zhou, S., Higgins, W., Zou, C.-Z., Liu, Q., Chen, Y., Han, Y., Cucurull, L., Reynolds, R. W., Rutledge, G. & Goldberg, M. 2010 The NCEP climate forecast system reanalysis. *Bulletin of the American Meteorological Society* **91**, 1015–1058. https://doi.org/10.1175/2010BAMS3001.1.

Serrat-Capdevila, A., Valdes, J. B. & Stakhiv, E. Z. 2014 Water management applications for satellite precipitation products: synthesis and recommendations. *Journal of the American Water Resources Association* **50**, 509–525. https://doi.org/10.1111/jawr.12140.

Setti, S., Rathinasamy, M. & Chandramouli, S. 2018 Assessment of water balance for a forest dominated coastal river basin in India using a semi distributed hydrological model. *Modeling Earth Systems and Environment* **4** (1), 127–140. https://doi.org/10.1007/s40808-017-0402-0

Setti, S., Maheswaran, R., Radha, D., Sridhar, V., Barik, K. K. & Narasimham, M. L. 2020a Attribution of hydrologic changes in a tropical river basin to rainfall variability and land-use change: case study from India. *Journal of Hydrologic Engineering* **25**, 05020015. https://doi.org/10.1061/(ASCE)HE.1943-5584.0001937.

Setti, S., Maheswaran, R., Sridhar, V., Barik, K. K., Merz, B. & Agarwal, A. 2020b Inter-comparison of gauge-based gridded data, reanalysis and satellite precipitation product with an emphasis on hydrological modeling. *Atmosphere* **11**, 1252. https://doi.org/10.3390/atmos11111252.

Shah, H. L. & Mishra, V. 2016 Uncertainty and bias in satellite-based precipitation estimates over Indian subcontinental basins: implications for real-time streamflow simulation and flood prediction. *Journal of Hydrometeorology* **17**, 615–636. https://doi.org/10.1175/JHM-D-15-0115.1.

Shayeghi, A., Azizian, A. & Brocca, L. 2020 Reliability of reanalysis and remotely sensed precipitation products for hydrological simulation over the Sefidrood River Basin, Iran. *Hydrological Sciences Journal* **65**, 296–310. https://doi.org/10.1080/02626667.2019.1691217.

Shukla, A., Ojha, C., Singh, R., Pal, L. & Fu, D. 2019 Evaluation of TRMM precipitation dataset over himalayan catchment: the upper Ganga Basin, India. *Water* **11**, 613. https://doi.org/10.3390/w11030613.

Singh, T. P., Kumbhar, V., Das, S., Deshpande, M. M. & Dhoka, K. 2020 Comparison of TRMM multi-satellite precipitation analysis (TMPA) estimation with ground-based precipitation data over Maharashtra, India. *Environment, Development and Sustainability* **22**, 5539–5552. https://doi.org/10.1007/s10668-019-00437-x.

Sunilkumar, K., Narayana Rao, T., Saikranthi, K. & Purnachandra Rao, M. 2015 Comprehensive evaluation of multisatellite precipitation estimates over India using gridded rainfall data. *Journal of Geophysical Research: Atmospheres* **120**, 8987–9005. https://doi.org/10.1002/2015JD023437.

Suseno, D. P. Y. & Yamada, T. J. 2020 Simulating flash floods using geostationary satellite-Based rainfall estimation coupled with a land surface model. *Hydrology* **7**, 9. https://doi.org/10.3390/hydrology7010009.

Tam, T. H., Abd Rahman, M. Z., Harun, S., Hanapi, M. N. & Kaoje, I. U. 2019 Application of satellite rainfall products for flood inundation modelling in Kelantan River Basin, Malaysia. *Hydrology* **6**, 95. https://doi.org/10.3390/hydrology6040095.

Tan, M. L. & Santo, H. 2018 Comparison of GPM IMERG, TMPA 3b42 and PERSIANN-CDR satellite precipitation products over Malaysia. *Atmospheric Research* **202**, 63–76. https://doi.org/10.1016/j.atmosres.2017.11.006.

Tang, X., Zhang, J., Gao, C., Ruben, G. B. & Wang, G. 2019 Assessing the uncertainties of four precipitation products for swat modeling in Mekong River Basin. *Remote Sensing* **11**, 304. https://doi.org/10.3390/rs11030304.

Tarnavsky, E. & Bonifacio, R. 2020 Drought Risk Management Using Satellite-Based Rainfall Estimates. pp. 1029–1053. https://doi.org/10.1007/978-3-030-35798-6_28.

Tesfagiorgis, K., Mahani, S. E., Krakauer, N. Y. & Khanbilvardi, R. 2011 Bias correction of satellite rainfall estimates using a radar-gauge product – a case study in Oklahoma (USA). *Hydrology and Earth System Sciences* **15**, 2631–2647. https://doi.org/10.5194/hess-15-2631-2011.

Thakur, M. K., Kumar, T. V. L., Narayanan, M. S., Kundeti, K. R. & Barbosa, H. 2020 Analytical study of the performance of the IMERG over the Indian landmass. *Meteorological Applications* **27**. https://doi.org/10.1002/met.1908.

Try, S., Tanaka, S., Tanaka, K., Sayama, T., Oeurng, C., Uk, S., Takara, K., Hu, M. & Han, D. 2020 Comparison of gridded precipitation datasets for rainfall-runoff and inundation modeling in the Mekong River Basin. *PLoS ONE* **15**, e0226814. https://doi.org/10.1371/journal.pone.0226814.

Tuo, Y., Duan, Z., Disse, M. & Chiogna, G. 2016 Evaluation of precipitation input for SWAT modeling in alpine catchment: a case study in the Adige river basin (Italy). *Science of The Total Environment* **573**, 66–82. https://doi.org/10.1016/j.scitotenv.2016.08.034.

Venkata Rao, G., Venkata Reddy, K., Srinivasan, R., Sridhar, V., Umamahesh, N. V. & Pratap, D. 2020 Spatio-temporal analysis of rainfall extremes in the flood-prone Nagavali and Vamsadhara Basins in eastern India. *Weather and Climate Extremes* **29**, 100265. https://doi.org/10.1016/j.wace.2020.100265.

Wang, J., Liu, G. & Zhu, C. 2020 Evaluating precipitation products for hydrologic modeling over a large river basin in the Midwestern USA. *Hydrological Sciences Journal* **65**, 1221–1238. https://doi.org/10.1080/02626667.2020.1737868.

Xie, P. & Xiong, A.-Y. 2011 A conceptual model for constructing high-resolution gauge-satellite merged precipitation analyses: GAUGE-SATELLITE MERGED PRECIP ANALYSIS. *Journal of Geophysical Research* **116**. https://doi.org/10.1029/2011JD016118.

Xue, X., Hong, Y., Limaye, A. S., Gourley, J. J., Huffman, G. J., Khan, S. I., Dorji, C. & Chen, S. 2013 Statistical and hydrological evaluation of TRMM-based Multi-satellite Precipitation Analysis over the Wangchu Basin of Bhutan: are the latest satellite precipitation products 3b42v7 ready for use in ungauged basins? *Journal of Hydrology* **499**, 91–99. https://doi.org/10.1016/j.jhydrol.2013.06.042.

Yeditha, P. K., Kasi, V., Rathinasamy, M. & Agarwal, A. 2020 Forecasting of extreme flood events using different satellite precipitation products and wavelet-based machine learning methods. *Chaos* **30**, 063115. https://doi.org/10.1063/5.0008195.

Yeggina, S., Teegavarapu, R. S. V. & Muddu, S. 2020 Evaluation and bias corrections of gridded precipitation data for hydrologic modelling support in Kabini River basin, India. *Theoretical and Applied Climatology* **140**, 1495–1513. https://doi.org/10.1007/s00704-020-03175-7.

Yu, C., Hu, D., Duan, X., Zhang, Y., Liu, M. & Wang, S. 2020 Rainfall-runoff simulation and flood dynamic monitoring based on CHIRPS and MODIS-ET. *International Journal of Remote Sensing* **41**, 4206–4225. https://doi.org/10.1080/01431161.2020.1714779.

Yuan, F., Zhang, L., Win, K., Ren, L., Zhao, C., Zhu, Y., Jiang, S. & Liu, Y. 2017 Assessment of GPM and TRMM multi-Satellite precipitation products in streamflow simulations in a data-sparse mountainous watershed in Myanmar. *Remote Sensing* **9**, 302. https://doi.org/10.3390/rs9030302.

Yuan, F., Zhang, L., Soe, K., Ren, L., Zhao, C., Zhu, Y., Jiang, S. & Liu, Y. 2019 Applications of TRMM- and GPM-Era multiple-satellite precipitation products for flood simulations at sub-daily scales in a sparsely gauged watershed in Myanmar. *Remote Sensing* **11**, 140. https://doi.org/10.3390/rs11020140.

Zhang, T., Yang, Y., Dong, Z. & Gui, S. 2021 A multiscale assessment of three satellite precipitation products (TRMM, CMORPH, and PERSIANN) in the three gorges reservoir area in China. *Advances in Meteorology* **2021**, 9979216.

Zhu, D., Wang, G., Ren, Q. & Ilyas, A. M. 2020 Hydrological evaluation of hourly merged satellite–station precipitation product in the mountainous basin of China using a distributed hydrological model. *Meteorological Applications* **27**. https://doi.org/10.1002/met.1909

First received 21 April 2022; accepted in revised form 11 November 2022. Available online 2 December 2022